Science Progress (2011), 94(4), 339–413
doi: 10.3184/003685011X13130481780217

Electron spin resonance. Part two: A diagnostic method in the environmental sciences

CHRISTOPHER J. RHODES

ABSTRACT

A review is presented of some of the ways in which electron spin resonance (ESR) spectroscopy may be useful to investigate systems of relevance to the environmental sciences. Specifically considered are: quantititave ESR, photo-catalysis for pollution control; sorption and mobility of molecules in zeolites; free radicals produced by mechanical action and by shock waves from explosives; measurement of peroxyl radicals and nitrate radicals in air; determination of particulate matter, polyaromatic hydrocarbons (PAH), soot and black carbon in air; estimation of nitrate and nitrite in vegetables and fruit; lipid-peroxidation by solid particles (silica, asbestos, coal dust); ESR of soils and other biogenic substances: formation of soil organic matter, carbon capture and sequestration (CCS) and no-till farming; detection of reactive oxygen species in the photosynthetic apparatus of higher plants under light stress; molecular mobility and intracellular glasses in seeds and pollen; molecular mobility in dry cotton; characterisation of the surface of carbon black used for chromatography; ESR dating for archaeology and determining seawater levels; measurement of the quality of tea-leaves by ESR; green-catalysts and catalytic media; studies of petroleum (crude oil); fuels; methane hydrate; fuel cells; photovoltaics; source rocks; kerogen; carbonaceous chondrites to find an ESR-based marker for extraterrestrial origin; samples from the Moon taken on the Apollo 11 and Apollo 12 missions to understand space-weathering; ESR studies of organic matter in regard to oil and gas formation in the North Sea; solvation by ionic liquids as green solvents, ESR in food and nutraceutical research.

Keywords: *quantititave ESR, photo-catalysis, zeolites, explosives, peroxyl radicals, nitrate radicals, particulate matter, PAH, asbestos, coal dust, photosynthesis, fuel cells, photovoltaics, kerogen, carbonaceous chondrites, nutraceutical research*

Professor Chris Rhodes has a visiting position at the University of Reading and is Director of Fresh-lands Environmental Actions. He has catholic scientific interests (www.fresh-lands.com) which cover radiation chemistry, catalysis, zeolites, radioisotopes, free radicals and electron spin resonance spectroscopy, which more recently have developed into aspects of environmental decontamination and the production of sustainable fuels. Chris has given numerous radio and televised interviews concerning environmental issues, both in Europe and in the United States – including on BBC Radio 4's Material World. Latest invitations include a series of international Café Scientifique lectures regarding the impending depletion of world oil and the need to develop oil-independent, sustainable societies. He has published more than 200 peer-reviewed scientific articles and five books. He is also a published novelist, journalist and poet. His novel ''University Shambles'' has just been released as an eBook and has been nominated for Brit Writers' Awards 2011: Published Writer of the Year. E-mail: cjrhodes@fresh-lands.com

1. Introduction

The present review is a companion to a related survey published in a previous issue of Science Progress entitled, ''Electron spin resonance: a diagnostic method in the biomedical sciences[1] '', and extends its coverage into the application of ESR to the many and various aspects of the environmental sciences. In reality, there is an element of overlap and certain topics could legitimately have been included in either review, since various environmental factors do indeed influence human health and hence are of relevance to the biomedical sciences. Therefore, while trying to avoid too much duplication, I reiterate the following essentials of the method *per se*, of which a more detailed coverage may be found in the first review[1]. Electron spin resonance (ESR) – also known as electron paramagnetic resonance (EPR) – tends to receive far less coverage than its relative, nuclear magnetic resonance (NMR). This is partly because NMR spectrometers and their uses are more ubiquitous, and furthermore, unless there is a specialist in the subject on the staff, ESR receives only scant mention in university science courses. In principle, NMR spectra may be recorded from dozens of different nuclei, whereas obtaining an ESR spectrum requires some of the sample molecules to contain one or more unpaired electrons, which might appear to be a curiosity feature. Nonetheless, here lies the real crux of ESR, since the method is completely specific for unpaired electrons, which are frequently formed in materials that have encountered one or more of a range of important energetic conditions, for which a signature is supplied in the form of the consequent ESR spectrum. The unpaired electron-bearing

sites are usually termed ''damage centres'', ''defects'' or ''trapped electrons'' by physicists, geologists, archeologists and environmental scientists, but are normally referred to by chemists and biologists as ''free radicals'', whose detailed molecular structures may be revealed from the spectral parameter of hyperfine splitting, where it is observed, and that of the g-factor.

Paramagnetic transition-metal cations, Fe^{3+}, Mn^{2+}, Cu^{2+}, are quite commonly detected in environmental samples and in biological tissues using ESR. Paramagnetic materials, including metal cations and synthesised complexes or stable organic radicals (usually nitroxides), may be deliberately added to samples as probes of local molecular environments such as cell-membranes, and to determine their dynamic properties. Along with other stable ''organic'' radicals (carbon chars and lithium phthalocyanines), nitroxides may be used to measure oxygen tensions in a variety of ''soft'' materials including foodstuffs. When it is desired to investigate various reacting systems for the intermediacy of free radicals, ''spin-traps'' are often added. These are frequently of a structural type designed to ''trap'' reactive radicals by addition to them, so forming nitroxides *in situ*, which give rise to detectable concentrations in consequence of their relative stability. Clearly, there are many and varied important applications for ESR, and most importantly so in areas of the biological and environmental sciences.

Unpaired electrons are created in a broad variety of samples which have often encountered fairly extreme conditions; high-energy (ionising) radiation (X-rays, γ-rays), energetic particles (electrons, protons, α-particles), UV light, high temperatures, combustion processes, reactive chemical reagents, mechanical stress, explosions. As we shall see, under both these and other sets of conditions, structural dislocations may be introduced in the form of organic and inorganic free radicals, which host unpaired electrons, and their ESR signal may provide a marker of the kind of process which has created them. The great power of ESR is its ability to identify the chemical nature of free radical species, and from the intensity of the signal, the number of radicals that have been formed in particular systems. From the line-widths and line-shapes of the ESR spectra from radical species, frequently as deliberately introduced to samples as spin-probes, various features of the local molecular environment may further be deduced. For example, details of the local molecular environment and phase-transitions in such complex media as foodstuffs (ice-cream and dough) may be deduced using spin-probes as additives.

Free radicals, moreover, play a central role in nature, particularly in living systems, and consequently, current activity in researching into these species is enormous. Mainly, this is because it is widely held, in part through the agency of ESR measurements, that radicals provide both the cause and mediation of many diseases, and indeed of the ageing process itself. The generally reactive character of radicals and unpaired-electron species overall (including metal ions, which can participate in redox processes) further underpins much of chemistry (it is, of course, ''chemistry'' which is implicit to all the above), and it is largely on the findings from simpler chemical systems that much of current biochemical thinking is based, and this underlying free radical chemistry impacts further on a variety of environmental aspects – especially in the role of pollutants in atmospheric phenomena, such as ozone-loss, global warming and acid-rain production. Furthermore, since the atmosphere is in direct contact and exchange with the surface of the Earth – with the soil, the plants which grow within and upon it (biosphere), the rocks and mountains (lithosphere), and the rivers, seas and oceans (hydrosphere) – the atmospheric chemistry takes-on a wider role. Remarkably, ESR can provide insight into many of these phenomena too, both through its use in the investigation of model systems, and more directly as an analytical technique.

2. Quantitative ESR ("Q-ESR")

Since many of the applications to be described in which ESR is used as an analytical technique involve the measurement of the unpaired electron concentration (also known as the spin-concentration or spin-count) in samples, it appears appropriate to discuss this at the outset. Obtaining reliable measurements of ESR signal intensities is extremely tricky[2], and it almost appears that all vital aspects of the ESR experiment act in conspiracy against managing this successfully. For a start, the sensitivity of the measurement depends acutely on the position of the sample in the microwave cavity, and is greatest at a single point at the cavity centre. On moving the sample away from this point, in any direction, the ESR signal intensity is found to decrease. The sample tube can be constrained by means of a ''collet'', so that movement only up and down in the cavity is possible.

When the sample is a liquid (and therefore is homogeneous), potential problems in its positioning may be circumvented by using a completely filled sample-tube which extends through the

full length of the cavity. In this case, the exact position of the sample has far less influence on the signal intensity, provided that the sample-tube is homogeneous in its diameter and wall-thickness. This approach was used in the study of relative antioxidant efficiencies[3]. For many solid materials, it is not possible to provide a *homogeneous*, cavity-length sample. Therefore, the sample position needs to be determined precisely. Various devices have been devised for this purpose; the simplest being merely to draw a calibration mark on the sample tube, so that its penetration-depth through the collet and into the cavity is known and is consistent. For a series of samples, a set of matched tubes is required, each calibrated to the same depth, which ideally brings the sample to the cavity centre, in order to maximise sensitivity.

For quantitative comparisons between samples, they should be as closely matched in composition as possible. This applies to the use of standard samples against which may be measured unpaired electron concentrations: these are more usually referred to as ''spin concentrations'', and are quoted as the number of ''spins'' (unpaired electrons) per gram of sample. [As a ''rule-of-thumb'', it is often said that a typical X-band ESR spectrometer can detect down to *ca* 10^{13} ''spins'' per gram, but the actual achievable value depends on all kinds of things!]. So, at the very least, the sample tubes should all be filled to the same depth, and at best, the standard should consist of the same material as the sample. Since this is rarely possible, a more practical alternative strategy is to match the materials as closely as possible in their dielectric properties. For example, in quantifying the amount of elemental carbon (EC) and organic carbon (OC) (mainly polyaromatic hydrocarbons; PAH) in particles sampled from the air in Sofia (Bulgaria), Yordanov and his coworkers have prepared a set of standards by dispersing a synthetic carbon–Char in talc[4], since the dominant sample component is of similar mineral (silicate) type. [In sampling air from the Mersey Road Tunnel, in Liverpool, we found that silica powder serves the same purpose.]

Finally, of course, the operating conditions of the ESR spectrometer, gain, modulation and microwave power level, should be the same for both sample and standard, although the signal intensity response to the *gain* is probably sufficiently linear to permit extrapolation from one sensitivity range to another, as is required when the two specimens have widely different spin-concentrations. The construction of the cavity has also been shown as critical in Q-ESR measurements[5].

2.1 Standards

Strictly, the spin concentration should be determined against a standard and, in principle, any paramagnetic material of known spin concentration might be used. In practice, DPPH (1,1-diphenylpicrylhydrazyl) is widely used. The spin concentration of the standard is determined from the quantity (number of molecules) present, and a corresponding ''area'' under the absorption peak is obtained by double integration of the first-derivative spectrum. Then the sample is run, the spectrum is also double integrated, and from the relative areas, the spin concentration of the sample may be deduced. This is not always necessary, and good results may be achieved on the basis of relative peak heights alone. Yordanov and his group have constructed a special sample holder, into which a sample of Mn^{2+} is strategically sealed[6]. By varying the relative height of the sample holder in the cavity, and of the sample within the holder, relative heights of sample/Mn^{2+} signals may be obtained, which give very good linear correlations, and which seem to be more reliable than using a full ''spin-count''. It is also thought that this approach offsets the loss of power of the klyston, which occurs inevitably over time, since both sample and Mn^{2+} signals will be equally affected.

3. ESR studies of photo-catalysis for pollution-control

Considerable efforts have been made to optimise photo-catalytic systems for use in cleaning water of organic pollutants[7–10]. The essential requirement is that the solution should be air-saturated, and contain suspended particles of a semiconductor to serve as the photo-catalyst, one such material being titanium dioxide. When TiO_2 (or indeed any other semiconductor) is irradiated with light, electrons are promoted from the valence band (vb) to the conduction band (cb) of the material. The ''band-gap'' (excitation energy) for TiO_2 is 3.2 eV, which corresponds to a wavelength of *ca* 400 nm, and is at the border of the UV-Vis spectrum. The process generates positive holes (electron vacancies) in the valence band (h_{vb}^{+}) and electrons (e_{cb}^{-}) in the conduction band. A number of events may then occur, which result in the formation of reactive species capable of reacting with and decomposing any organic pollutants that may be present. The initial species (h_{vb}^{+}) and (e_{cb}^{-}) can either react directly with the organic agents as sorbed on the surface of the

particle, or they may be converted into reactive intermediates which react with the organic pollutants either directly on the surface or close to it. In the case of TiO_2, it is normally thought that (h_{vb}^+) is transformed into hydroxyl radicals (·OH) by the oxidation of H_2O, while, in the presence of molecular oxygen, (h_{cb}^-) forms the superoxide radical anion ($O_2^{-\cdot}$), which serves to leave the holes free to react. The limiting factor in determining the efficiency of the photo-catalytic process is the rate of recombination of (h_{vb}^+) and (e_{cb}^-), in competition with the formation of other reactive species, of which ·OH radicals are believed to be the major agents responsible for the decomposition (''mineralisation'') of organic pollutants (Figure 1) [11,12], since they are fiercely oxidising. Indeed, compelling evidence has been gleaned from ESR spin-trapping studies that ·OH radicals are produced on light irradiation of aqueous solutions containing TiO_2.

The ·OH radical trapping efficiency by DMPO (5,5-dimethyl-1-pyrroline-N-oxide) has been estimated as *ca* 33%[13], and so, in principle, might be used to estimate the yield of ·OH radicals in a photo-catalytic system; however, a much improved value of *ca* 80% was demonstrated by trapping ·OH with the stable free-radical 3-*carboxyproxyl* (3-carboxy-2,2,5,5-tetramethylpyrrolidine-N-oxyl), a reaction that leads to the diamagnetic product proxyl-NH (3-carboxy-2,2,5,5-tetramethylpyrrolidine)[14]. Therefore, the latter is the better method. The main difference between the two methods is that, in the spin-trapping procedure, the appear-

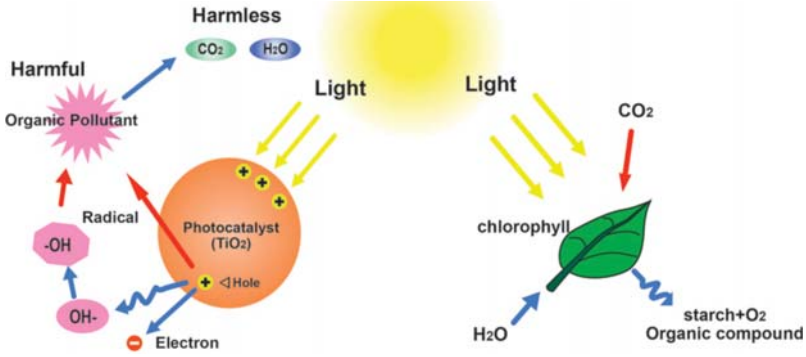

Figure 1 *Absorption of light by TiO_2 particle, with the generation of positive holes and electrons. The holes can oxidize water to form* ·OH *radicals, while the electrons are scavenged by O_2 molecules to form superoxide radical anions ($O_2^{\dot{U}\cdot}$), both of which can mineralise organic pollutants by oxidation. Reproduced with permission. http://www.airrevolution.co.za/research.html*

ance of the spin-adduct of DMPO/·OH is monitored, while the latter measurement relies upon the disappearance of the initial signal from 3-*carboxyproxyl*, as it scavenges ·OH radicals. It is thought that this occurs by an initial coupling of the two radical species, followed by elimination of O_2 from the primary product, proxyl-NOOH, to give proxyl-NH which is the species mainly isolated (along with minor amounts of proxyl-NOH). From a measurement of the line heights and widths, a rotational correlation time of 38 picoseconds was deduced for 3-carboxyproxyl in water, which increased to 45 picoseconds when TiO_2 was added: although this change is not large, it does indicate some interaction between the probe and the catalyst surface. The rate of formation of ·OH radicals was found to be a linear function of the light intensity at low intensities, and serves as a mechanistic parameter with which to investigate the mechanism of formation of this reactive species by the photo-excitation of TiO_2 [14].

4. Studies of zeolites

Zeolites have a profound ability to absorb molecules of water and of many other substances. Zeolites contain small holes (micropores), which are generally of less than 13 Å in diameter, and hence of molecular dimensions, and it is into these that molecules are actually absorbed. The essential framework of a zeolite is an aluminosilicate which carries an overall negative charge. This is counterbalanced by the presence of metal cations[15–17]. In consequence, zeolites can be used as ion-exchangers, and may be used to ''soften'' water, since cations such as Ca^{2+} and Mg^{2+} which make water ''hard'' are absorbed into the zeolite, while H^+ or Na^+ originally present are displaced. Of greater importance is that radioactive cations, particularly Sr^{2+} and Cs^+ [17], can be removed from the cooling water output produced during the operation of nuclear power plants (NPPs), in order to minimise their contaminating the environment in the first place, and in remedial clean-up operations when radioactive material has inadvertently been released. Indeed, around 500,000 tonnes of zeolites were used in the aftermath of the disaster at Chernobyl in 1986, supplied from mines across the former USSR[18]. Zeolites have many and various important environmental applications, as has been summarised[17].

- Buildings: four million tonnes of natural zeolites are mined annually

mainly to be used in the construction industry, of which 2.5 million tonnes are shipped to China to make a light-weight concrete. Volcanic tuff may be cut with handsaws and used directly to fabricate houses and indeed all kinds of buildings, in regions where it is plentiful, Republic Square in Yerevan, Armenia, with its architectural splendour.

- Around 1.4 million tonnes of zeolite A are synthesised each year for use as a ''builder'' in detergents, to remove and encapsulate Ca^{2+} and Mg^{2+} cations which make water ''hard'', rather than polyphosphates which cause algal bloom in lakes and rivers.
- Toxic heavy metal cations, Pb^{2+}, Cd^{2+}, Zn^{2+}, may also be removed from the environment by cation-exchange into zeolites.
- Toxic anions may also be removed by reaction with heavy metal cations previously exchanged into the zeolite. For example, a silver-exchanged zeolite can be used for removing radioactive iodine (iodide ions) in the form of insoluble AgI which stays in the zeolite. Other toxic anions: cyanide, arsenite, arsenate, chromate and molybdate may similarly be removed so long as the precipitated salt has a sufficiently small solubility product.
- H^{+}-exchanged zeolites, ultrastable zeolite Y (USY) are used as solid acid catalysts in the petrochemical industry. Around 300,000 tonnes of synthetic zeolites are manufactured annually for his purpose.
- Ni^{2+} exchanged zeolites have been demonstrated to absorb sulfur compounds (thiophene derivatives and thiols) from model ''diesel'' in accord with a desire to to reduce transportation-based SO_2 emissions, and hence the damaging effects of ''acid rain'' on rivers and the facades of buildings.
- Reduction in NO_x emissions from vehicles, using zeolite-loaded ''catalytic converters''.
- Surfactant-modified zeolites have a potential to remove toxic anions, chromate *and* organic pollutants, trichloroethylene, simultaneously from the environment. It is common that a region is co-contaminated with a mixture of pollutants and such a multifunctional decontamination agent might be very useful. Contaminated groundwaters are a good example.
- Molecular sieves: small-pore zeolites (such as zeolite-A) selectively absorb small polar molecules, water, and so zeolite ''molecular sieves'' are highly efficient drying agents for removing traces of water from other solvents.
- Hydrocarbon sieving: linear n-alkanes (needed to make detergents) can be separated from branched alkanes, since the former pass more slowly through a column packed with zeolite 5A in consequence of

their preferential penetration of the zeolite pores, which results in a more tortuous passage through the material. Millions of tonnes of n-alkanes are produced annually by this method.

- H^+-exchanged zeolites (H-ZSM-5) are used as solid acid catalysts, for ''cracking'' in the petrochemical industry.
- Medical applications: Hemosorb and QuikClot are commercial products based on zeolites which when applied to wounds (occasioned in accidents, battle-field situations or by surgery) are said to cause an ''instant'' cessation of bleeding. Zeolites are also used in kidney dialysis machines, to absorb ammonia from blood and prevent it from building up in the body (a job that healthy kidneys normally do).
- Separation of gases: there are commercial units that can provide oxygen of 95% purity for use in hospitals or for patients, those suffering from emphysema and other forms of obstructive pulmonary disease (OPD), by separating it from air. Nitrogen (80% of air) is preferentially absorbed over oxygen by a zeolite because of its much larger molecular electric quadrupole moment, and so enables oxygen to separate from air almost in a state of purity.
- Agriculture: for supplying K^+ and $NH_4{}^+$ to plants from soils that have been enriched with zeolites exchanged specifically with these cations. It is suggested that such ''zeoponics'', as the strategy is called, might be used to grow food on long space missions, if we ever send ''a man to Mars''.
- Contaminated, brown field land may be rendered fit for building and even for agriculture by treating the soil with sufficient quantities of zeolites, which remove heavy-metal cations.
- Use in more efficient heating systems. Essentially, the adsorbed water can be driven out of a zeolite by heat, but when the water is readsorbed, heat is given out. The principle can be incorporated into a heat-pump system which uses more of the available energy for actual heating, most of which would otherwise be wasted.

ESR has proved its utility in elucidating many essential properties of molecular adsorption, mobility of contained molecules and catalysis by zeolites, as is illustrated in the following examples.

4.1 Studies of liquids sorbed in zeolites using ESR

Different kinds of materials may be used, including nitroxides, to probe the motional behaviour of a liquid: this is often different for the material in bulk form or as confined in micro-pores[19]. In general, it is found that the differences vary markedly according

to pore size, but depend less on the nature of the porous material (whether it is, say, a silica-gel or a zeolite). Since zeolites contain cations that occupy particular sites in an overall negatively charged porous framework, further differences are expected according to the charge-state of the nitroxide probes, which are available (Scheme 1) in neutral, cationic or anionic forms, the spin probes, 4-Hydroxy-TEMPO (TEMPOL), CAT-1 (Temp-TMA^+) and and $TEMPYO^-$ ($Tempyo^-$).

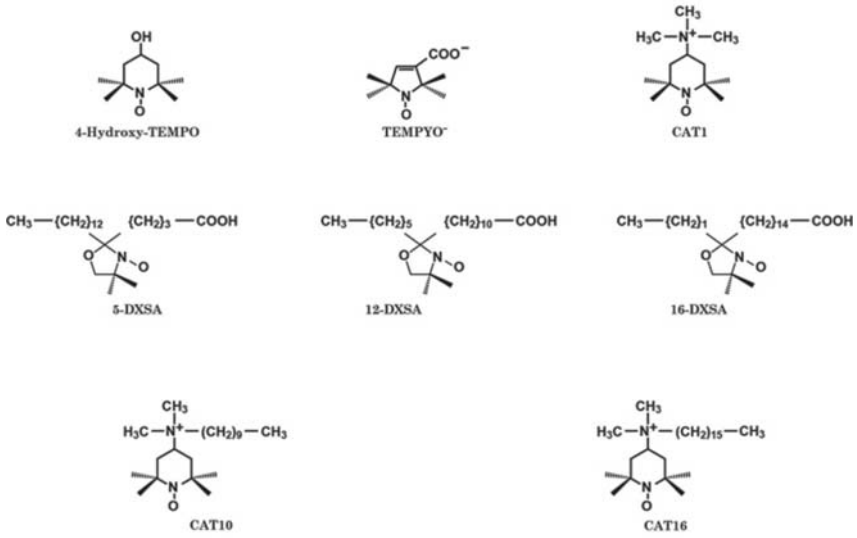

Scheme 1 *Structures of the nitroxide spin-probes discussed in the text.*

In one example, each of the three probes was sorbed[20], as a 4×10^{-4} M solution in ethanol, into samples of the synthetic zeolite NaX (13X) which had been deprived of water by heating at 200°C under vacuum for 3–4 h. ESR spectra were recorded in the temperature range 138–298 K both for solutions in bulk form and as sorbed into the zeolite. For TEMPOL, the sharp ''three-line'' spectrum of the probe undergoing ''fast-motion'' persisted down to 160 K in the bulk solution, below which spectra characteristic of ''slow-motion'' were recorded; this transition occurred at a rather higher temperature of 180 K in the micro-pore contained solution. Temp-TMA^+ displayed the transition below 180 K in bulk ethanol, but as sorbed in 13X, although a sharp ''three-line'' pattern appeared above 210 K, it remained superimposed on the signal from an immobilised fraction which persisted up to room temperature. In the sorbed situation, the mobility of the probe decreases in the order: $Tempyo^- > TEMPOL > Temp\text{-}TMA^+$, in line with

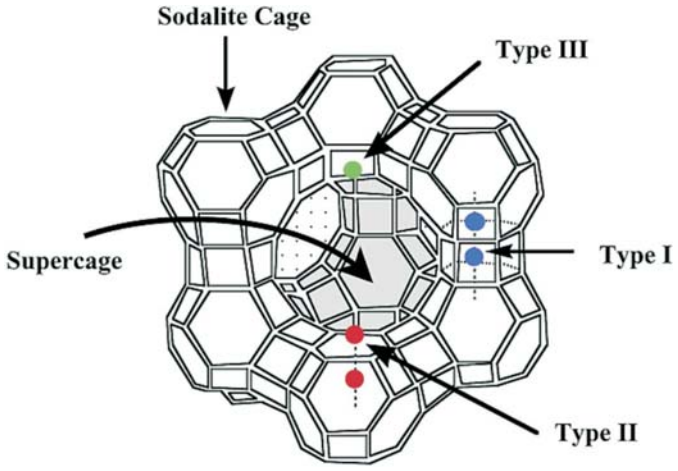

Figure 2 *Structure of faujasite showing central supercage surrounded by sodalite cages, along with cation sites. Reproduced with permission from Professor N.J. Turro. http://turmac13.chem.columbia.edu/images/publications/NJT728.gif*

increasingly strong interactions with the zeolite surface. The interesting observation of two distinct motional regimes for Temp-TMA^+ is interpreted in terms of probe molecules which are located at different sorption sites in separate cavities. [The absence of line broadening immediately excludes that two such molecules are present together in the same cavity]. Distinct cation

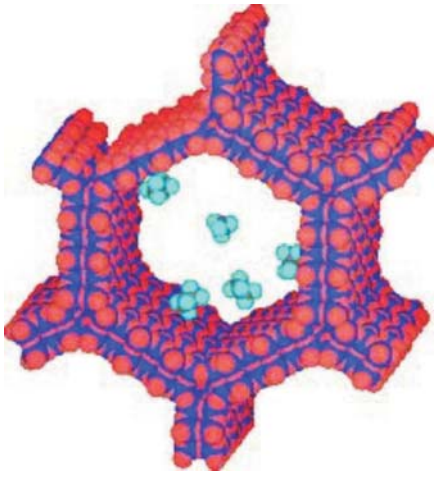

Figure 3 *Methane and ethane adsorbed inside one of the hexagonal pores of MCM-41, which is* ca *3 nm in diameter. Reproduced with permission. http://www.chm.bris.ac.uk/motm/mcm41/mcm41.htm*

sites are well established in fuajasites[15–17], such as zeolite X and zeolite Y, and are called simply site II and site III (Figure 2), and so it is not surprising that the cationic probe molecules would seek these out. A species sorbed thereon might be expected to give slow-motion spectra, whereas a probe free to move within the cavity fluid should give fast-motion spectra. Clearly any exchange of Temp-TMA^+ molecules between sites II and III and the cavity fluid occurred slowly enough to give separate ESR absorptions. For linewidths of the order of 1–2 G, the exchange rate must be less than $(2-3) \times 10^7\ s^{-1}$.

MCM-41 (mobil crystalline material) is an ordered mesoporous material (Figure 3), with a microporous structure of uniform mesopores (3 nm in diameter) running through a matrix of amorphous silica. As a working definition, micropores are those of less than 2 nm, while mesopores range in size from 2 to 50 nm. Pores larger than this are termed macropores. MCM-41 is highly porous (pore volume $> 1.0\ mL\ g^{-1}$) and has a high associated surface area ($1000\ m^2\ g^{-1}$). It is therefore of interest as a potential support material in fabricating heterogeneous catalysts, since it offers the possibility to provide highly dispersed catalytic phases. Unfortunately MCM-41 has a limited robustness in the presence of various reagents and there is an ongoing effort to introduce catalytically active phases, especially nickel/nickel oxide and molybdenum oxide, inside the mesopores of the material[21]. The effect of confinement on molecules in MCM-41 was investigated using a spin-probe as detected by ESR spectroscopy. When the solid was added to an aqueous solution of a nitroxide spin- probe, the initially sharp ESR spectrum was found to broaden, while a superimposed sharper signal remained as a minor component. It appears that MCM-41 traps the solute molecules within the nanochannels, which cause the solvent water molecules to form a relatively stable molecular cage. A detailed analysis of the ESR spectrum indicates that the nitroxide molecules undergo anisotropic reorientation without being physically adsorbed by the channel wall[22]. The mobility of 2-propanol and water molecules within the MCM-41 nanochannel as a function of temperature was further determined. The results demonstrate that two phases are formed by the 2-propanol molecules: in one the molecules are partially immobilised on the ESR lime scale (even at temperatures of 40 K above the bulk melting point of the pure material) along with a far more mobile second phase. Water, in contrast, showed only an ''immobilised'' phase even when the temperature was increased to 313 K. At higher temperatures still, the spin-probe molecules

undergo anisotropic rotational diffusion which reduces motional resistance from the solvent molecules in the nanochannel[23]. At high concentrations (30 mM), spin probes exhibit very broad ESR spectra from Heisenberg spin exchange. When the solution is encapsulated in the nanochannel of MCM-41, however, a much sharper spectrum is recorded, which suggests that collisions between the solute molecules within the nanochannel are quenched. Superimposed ESR patterns are detected: a sharp signal from the probe in the nanochannel and a broad spectrum from the bulk solution. When the system is cooled to temperatures in the range of 10–20 K above the melting point of the alcohol, the ESR spectrum from molecules within the nanochannel changes to that characteristic of a glassy state. A steady sharpening of the spectrum occurs as the temperature increases, and the glassy signature finally disappears at around 293 K. It may be that the solvent molecules form a liquid-crystalline-like structure involving hydrogen bonding which prevents the solute from undergoing translational diffusion within the nanochannel[24].

Aqueous solutions of di-tert-butyl nitroxide (DTBN) (Scheme 2) and 2,2,6,6-tetramethylpiperidine-1-oxyl-4-ol (4-Hydroxy-TEMPO) flowing in a quartz column of 0.81 mm internal diameter packed with well-dried MCM-41 were studied by ESR. In both cases, a very broad signal which accounts for >98% of the total is ascribed to spin-probe molecules that are located in the MCM-41 nanochannel, along with a minor sharp signal from probe molecules that occupy the bulk space between the MCM-41 particles.

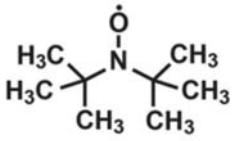

Scheme 2 *Structure of di-tert*-butylnitroxide (DTBN) spin-probe discussed in the text.

Although the spin probes are located deep in the cylindrical (3 nm diameter channel) nanospace of MCM-41, they are transported downstream fairly rapidly. It is concluded that the aqueous solution is transported through the nanochannel of MCM-41 relatively slowly but, nonetheless, more quickly than is predicted from conventional flow-considerations. With solutions of the same spin probes at high concentration in ethanol solution, the ESR spectra also show different spectral forms in the two spaces but the profiles are less distinct. Since the translational diffusion of the individual molecules is quenched in

the nanochannel, both the solute and solvent molecules must move collectively through it. It is proposed that this method with which to study the fluid flow in nanospaces may be called ''spin probe nano flowmetry'' [25]. In another study by this group, highly concentrated solutions of DTBN were condensed on several silica materials, such as MCM-41, two types of SBA-15, and fumed silica. At a very low level of doping only the ESR spectrum of an immobilised nitroxide radical is observed, but as more of the solution is adsorbed, the spectrum sharpens until a well-resolved three-line spectrum is observed, when sufficient of the solution has been added as is estimated to cover the surface with a monomolecular layer. Hence, the DTBN molecule can tumble rapidly on/in this solvent layer. As yet more solution is added, the ESR spectrum changes differently and characteristically from system to system: thus, the line-width increases in a practically linear fashion for the SBA-15 and fumed silica systems. However, in the case of MCM-41 it remains nearly constant until the quantity of solution added is greater than the total capacity of a nanochannel. The increase in line-width as more solution is added is small for the SBA-15 system but large for the fumed silica system. An interpretation is offered in terms of the structural geometry of their silica materials and with a condensation model for the alcohols on these surfaces. Furthermore, a model of the collective probe/solvent molecular flow of the alcohol solutions through the nanochannel of MCM-41 is derived[26].

4.2 Non-nitroxide spin-probes in zeolites

Lund and his co-workers have published a series of papers[27–29,31] on the structure and dynamics of nitrogen-containing radical cations, $R_3N^{+\cdot}$ and $R_3N^+ - \dot{C}H_2$, formed by radiolysis of zeolites containing adsorbed trialkylamine or (as synthesised) containing R_4N^+ as the organic template (a material that assists the crystallisation of the particular zeolite form). Even when the R_4N^+ cation is too large to enter the pores of a zeolite by standard cation-exchange procedures, it may be introduced *in situ* during the zeolite synthesis. The internal dynamics of the $Me_3N^+ - \dot{C}H_2$ radical cation as produced in γ-irradiated Al-offretite was investigated[27]. The spectra were strongly temperature dependent, within the interval of 4–300 K. From a spectrum measured at 110 K, the hyperfine splitting could be simulated using a dominant anisotropic coupling to two equivalent protons of *ca* 22 G (the CH_2 group), which is axially symmetric according to exchange of the protons by rotation about the N—CH_2 bond. Over the temperature range

employed, this changes little, nonetheless the initial substructure on each line of the 1 : 2 : 1 triplet of a 1 : 3 : 3 : 1 quartet (from an equivalent coupling to one proton from each of the methyl groups) changes from 4.6 G to a ''decet'' of splitting 1.5 G, from nine equivalent protons at 300 K. This effect is due to restricted rotation of the methyl groups, and can be analysed to yield an activation energy of 8.1 kJ mol^{-1}. The coupling to the ^{14}N nucleus is unchanged by the motional processes and remains at a constant 3.5 G[27]. The research was extended to a study of the influence of cage size/type using Al-offretite, SAPO-37 and SAPO-42 in their ability to stabilise the radical cations $Me_3N^{+\cdot}$ and $Me_3N^+ - \dot{C}H_2$ [28], in which the radicals were produced by γ-irradiation of these zeolites which all contained Me_4N^+ cations as the organic template. $Me_3N^{+\cdot}$ was stable at room temperature in the relatively small, sodalite, cages of SAPO-37 and in the β-cages of SAPO-42. $Me_3N^+ - \dot{C}H_2$ was also stable in the sodalite cages of SAPO-37, and also in the relatively large, gmelinite, cages or in the main channels of Al-offretite and in the α-cages of SAPO-42. The exchange rates of the methyl group hydrogen atoms in $Me_3N^+ - \dot{C}H_2$ are in the order: SAPO-37 (sodalite cages) < Al-offretite (gmelinite or the main channels) < SAPO-42 (α-cages), and follows the order of the relative cage sizes: sodalite (*ca* 6 Å) < the gmelinite cage (*ca* 6 × 7.4 Å) or main channels (*ca* 6.5 Å) < the α-cage (11 Å).

In a second paper[29], is reported an investigation of the structure and dynamic properties of the radical cations of triethylamine ($Et_3N^{+\cdot}$) and tripropylamine ($n - Pr_3N^{+\cdot}$), formed by exposure to γ-radiation of $AlPO_4$-5 in which the neutral precursor amines were incorporated as an organic template during synthesis. Both $Et_3N^{+\cdot}$ and $n - Pr_3N^{+\cdot}$ were stable in $AlPO_4$-5 up to room temperature, and gave well resolved spectra throughout the entire temperature range 4–300 K. The temperature dependent spectra were analysed using a two-site exchange model in which the two inequivalent β-CH_2 hydrogen atoms of the CH_3CH_2- or $(CH_3CH_2)CH_2$-groups mutually interchange their positions, becoming equivalent on the ESR timescale. The exchange rates were evaluated by computer simulations of the ESR lineshapes, and were found to increase by over two orders of magnitude, in the range $10^8 \times 10^7\ s^{-1}$ to $6.6 \times 10^9\ s^{-1}$, as the temperature increased from 110 K to 270 K. As expected, the fully averaged coupling constant (20 G) is close to half that measured for the frozen conformation (36 G) on a simple $\cos^2\Theta$ basis for β-protons. From appropriate Arrhenius plots of the exchange rates as a function of

temperature, energy barriers to internal rotation were determined at 9.1 and 11.4 kJ mol^{-1} for $Et_3N^{+\cdot}$ and $n-Pr_3N^{+\cdot}$ respectively. Density functional theory (DFT) calculations predicted energy barriers of 8.7 and 7.7 kJ mol^{-1}, respectively and it is thought that the discrepancy from the value deduced experimentally for $n-Pr_3N^{+\cdot}$ arises from interactions between the radical cations and the zeolite wall[29]. We note that a similar increase in the activation energy for the interconversion of the radical cation of 9-octalin (1,2,3,4,5,6,7,8-octahydronaphthalene) to 28 kJ mol^{-1} as adsorbed in the zeolite H-mordenite, from the value of 14 kJ mol^{-1} measured in liquid solution, according to dynamic simulations of its ESR spectra[30]. The last paper[31] in this interesting set of reports provides an overview of the above work, and furthermore reports experiments in which nitric oxide (NO) is used as a probe, which forms a dimeric $(NO)_2$ triplet state ($S=1$) species in Na zeolite-A. At 5 K an anisotropic interaction with a single Na^+ cation was observed for this species.

NO has been employed more generally as a probe molecule for cations present in zeolites[32,33]. For example[32] it is shown that ESR spectra of the NO mono-radical adsorbed on a zeolite surface is characterised by three g-tensor components. This is as expected since NO is electronically orbitally degenerate in an unperturbed condition, but such degeneracy may be removed by electrostatic interactions with its local environment, such as being adsorbed on a surface. A 1 : 1 : 1 triplet hyperfine splitting is resolved on the g_{yy} feature stemming from coupling to the ^{14}N nucleus. It is the g_{zz} g-tensor component which is especially sensitive to the local environment in the zeolite and provides a measure of the surface electrostatic field. Since the magnetic orbital-coupling along the molecular axis, which is responsible for the g_{zz} shift, occurs between the unpaired electron orbital and a *vacant* orbital, this is negative in respect to the free-spin value ($g=2$) and typically g_{zz} lies in the range 1.8–1.9. This is the opposite to the effect for the superoxide radical anion ($O_2^{-\cdot}$)–which has two more valence electrons than NO–in which the dominant coupling is with a filled orbital, hence with g_{zz} values that are greater than $g=2$. We shall see more in Section 4 about the adsorption of homonuclear diatomic gases in zeolites and the induction of infra red absorption bands from them, but we note that electrostatic fields in zeolites have been estimated from the IR spectra of adsorbed molecular oxygen (O_2), in which the field induces a dipole moment, and the intensity of the IR band at *ca* 1555 cm^{-1} from the O—O stretching vibration increases in proportion to the square of the magnitude of the molecular dipole.

ESR measurements of NO as a probe molecule may well provide an effective but complementary alternative. Automated simulation of ESR spectra are possible through a new procedure which facilitates the analysis of a series of closely related spectra, that from NO adsorbed in different zeolites[32]. Lund and his coworkers have made a review on ESR and ENDOR studies of NO, NO_2 and Cu^{2+} cations adsorbed in zeolites, based mainly on their own extensive work in this field[33]. The underlying purpose of this work is to understand the diffusion and bonding of NO, NO_2 and Cu^{2+} involved in the catalytic removal of NOx with Cu-zeolites. Translational motion of NO_2 in mordenite, ZSM-5 and K- and L-type zeolites could be investigated from an analysis of the temperature-dependent ESR spectra using the slow-motional ESR theory developed by Freed and his coworkers. The spectral broadening that became apparent at increasing temperatures can be explained by Heisenberg exchange between the NO_2 molecules as they diffuse along the zeolite channels. In Na-ZSM-5, the spin-exchange rate increased markedly as the Si/Al ratio increased, and is understandable if the major barrier to its diffusion is caused by the interaction between NO_2 and Na^+ cations. Another paper reports on the influence of different zeolite structures on the motional dynamics of NO_2 [34], as determined from ESR measurements, from which the following deductions could be made: (1) in zeolites with similar channel structures, the diffusion rate of NO_2 is proportional to the channel size, leading to an order of diffusion rates: Beta-type > ZSM-5 > ferrierite and L-type > mordenite; (2) the diffusion is faster in those zeolites that have multi-dimensional channels (Beta-type, ZSM-5 and ferrierite) than in those with uni-dimensional channels (L-type and mordenite).

Turro and his coworkers have generated benzyl and other related kinds of delocalised radicals in zeolites as probe molecules for these solids in relation to their role in reactivity. They have coined the term *supramolecular steric effects*, to describe phenomena which stabilise diphenylmethyl radicals (DPM) formed by photolysis of 1,1,3,3-tetraphenylacetone as adsorbed onto the surface of the MFI zeolite LZ-105 from a solution in isooctane. The solvent was evaporated in a stream of argon, leaving a loading of 0.3–0.5%, which is enough to fill all the holes on the LZ-105 surface with the ketone and yielding a supramolecular system termed 1@LZ-105[35]. On photolysis, DPM was formed. While the supramolecular effect could prevent the dimerisation of DPM to form 1,1,2,2-tetraphenylethane – a reaction which proceeds in solution at near diffusion-controlled rates – reaction of DPM with molecular oxygen was

possible, since it could diffuse into the zeolite. The signals from DPM persisted over several weeks if air was excluded, but the spectrum was immediately replaced by another one from peroxyl radicals, $RO_2^{\cdot}$, when air was admitted. Since the spectrum did not change appreciably over the temperature range -23 to $-150°C$, it was concluded that the species $DPMO_2^{\cdot}$ was immobilised by adsorption on the zeolite internal surface. By pumping the sample down to a vacuum of 5×10^{-5} mmHg, the spectrum of DPM was recovered by dissociation of the corresponding peroxyl radical; the latter could be recovered by further admission of air, and restored to DPM by pumping, as could be repeated several times, showing that the reaction is fully reversible. It is proposed that supramolecularly stabilised reactive intermediates might be used to explore extensive intramolecular reactivity, and in this regard, a contrast may be drawn between a supramolecularly isolated and a matrix isolated system. Thus, while a ''matrix'' impedes *all* reactions of a given intermediate, a supramolecular medium is more selective and allows considerable rotational and diffusional freedom. As an example of this, we see a complete preclusion of dimerisation for DPM radicals, however, a complete and reversible equivalent bimolecular reaction with O_2 is possible. Additionally, the usual subsequent bimolecular reaction between $DPMO_2^{\cdot}$ radicals, as is observed in solution for organic peroxyls, is restricted, since the ESR signal from the primary peroxyl species is persistent[35]. The term *supramolecular* may be taken to mean ''*one level up from* [the] *molecular*'', hence addressing the immediate environment within which the reactive molecules are occluded. The strategy has been used in a study of ''recombination stereoselectivity'' with which to probe magnetic isotope and magnetic field effects for the coupling of 1-phenylethyl radicals, as generated within the micropores of NaY type zeolites by the photolysis of *meso*- or *dl*-2,4-diphenylpentan-3-one, present as co-adsorbed with a chiral inductor (diethyl tartrate or ephedrine)[36]. The reactions were found to be little affected by an external magnetic field of 2,000 G, but the geminate radical recombinations were sensitive to intramolecular magnetic isotope effects, such that an enhanced enantiomeric excess (*ee*) was obtained for the ^{13}C isotopomeric radicals in all cases[36]. A range of persistent radicals was similarly studied as adsorbed ''on'' ZSM-5 zeolites, formed by photolysis of a range of substituted dibenzyl ketones[37]. The word ''on'', used in the title of the paper, is significant in that radicals formed on the external zeolite surface are not persistent if they are unable to diffuse into the interior, a matter that depends on the nature (''supramolecular structure'') of

the initial radical@zeolite complex and the diffusion and reaction dynamics of the radicals produced by photolysis, which determines whether they are stable for periods of seconds to many hours. In order for persistence to be obtained at all, the radicals must initially separate and diffuse apart, whether they are formed on the external surface or on the internal pore surface. If they are formed on the external surface, the radicals must diffuse to the internal surface into the supramolecular state, or if they are produced by photolysis of a ketone adsorbed at the internal surface, they must separate and become located by diffusion at regions some distance apart to avoid rapid radical coupling. Size/shape features are important factors in determining molecular adsorption capacity and diffusional properties of molecules hosted in zeolites, and accordingly the structures of the parent ketones and daughter radicals were selected to impose variable steric constraints on the properties of these molecules. Radicals which are confined to the external surface by steric factors are transient since they undergo rapid dimerisation reactions there. The persistence of radicals located at the inner surface is a result of inhibition of bimolecular radical combination or disproportionation reactions, and in order to benefit from such stabilisation this is where they must be able to diffuse to. As an example of the sensitivity of the approach, the presence of an *ortho* methyl group is sufficient to prevent diffusion of a benzyl radical to the internal surface. This is clear from the ESR spectra, which shows that only the ''unmethylated'' benzyl radical remains persistent following photolysis of a ketone that must give this, along with a more hindered radical which is lost by reactions on the external surface. Analogous radicals with additional methyl substitution at the exocyclic positions show similar behaviour, which demonstrates that only those radicals that do not have an *ortho* ring-methyl group are persistent. Further extension of the alkyl chain apparently does not impede internal diffusion, since spectra from benzyl radicals bearing even exocyclic n-pentyl substituents are observed. Reactions of these persistent radicals with O_2 and NO were further investigated, and in the case of reaction with O_2, a high yield of persistent peroxyl radicals was observed. However, the addition of NO scavenges persistent benzyl-type radicals, which leads initially to the diamagnetic nitroso-adduct, which on further photolysis is transformed into a persistent nitroxide radical by subsequent radical trapping. A model is presented to account for the influence of structural variation in both the radicals and their parent ketones on their reactivities under the prevailing ''supramolecular'' conditions[37].

In one study, *ortho*-methyldibenzyl ketone, which is ESR silent, was co-adsorbed with an ESR detectable nitroxide spin-probe, for the purpose of characterising the external surface of silicalites, which possess MFI structures, but are made entirely of SiO_4 tetrahedra, in contrast to the ZSM-5 zeolites which contain aluminium centres (AlO_4^-), and exchange counter-cations. The external surface area of the silicalite (a practically all-silica ZSM-5 structure) can be related to the amount of ESR-silent co-adsorbate molecules required to attain a certain surface coverage by monitoring the change in the nitroxide ESR parameters, an increase in rotational freedom when some of the nitroxide molecules are displaced from the strong binding sites by the co-adsorbate molecules (which are characterised by ''powder'' type spectra). Isotopically labelled (^{15}N, ^{14}N) nitroxides were used and from the results obtained from them it was concluded that the molecules adsorbed on the strong binding sites are able to exchange efficiently with those in an isooctane solution or on the weak surface-binding sites on a time-scale of a few hours up to a day[38]. The supramolecular model derived from the photolysis of dibenzyl ketones adsorbed on zeolites is emphasised to take into account the effect of the physical and chemical nature of the structure of the zeolites and their effect on the radical species formed. Within this model are a number of phenomena including surface coverage, adsorption at internal and external surfaces, diffusion over the surfaces, molecular sieving of radicals, and the eventual product distributions. A novel method is introduced for ''titrating'' the binding sites via EPR spectroscopy. The influence of co-adsorbed spectator molecules of varying polarities, namely water, pyridine, and benzene, on the photolysis of *o*-methyldibenzyl ketone and dibenzyl ketone adsorbed on MFI zeolites is investigated. Insights are provided into a displacement mechanism prompted by the spectator molecules and further demonstrates how the product distribution of photolysis of sorbed ketones can be controlled[39].

Using an adaptation of a simple electrostatic model[40], combined with spin-populations derived from ESR measurements, the degree of $N(\delta^+)$—$O(\delta^-)$ charge separation in a nitroxide spin-probe (R_2N—$O^{\cdot}$) is equated with the surface electric fields in a series of cation-exchanged samples of zeolite-X: LiX, NaX, KX, MgX, CaX, SrX, BaX. Electric fields in the range $2.0-8.0\,V/A$ ($0.2-0.8\,V/nm$) are deduced[40], in good accord with values obtained from theoretical and other experimental procedures. The surface fields are of similar magnitude to those measured using the interaction between the molecular electric quadrupole of NO and zeolite

surfaces, according to the perturbation of the g-tensor[41]. We propose that the ESR/spin-probe method might be used very effectively in the estimation of a fundamental feature which underpins many of the properties and utilities of zeolites. The presence of metal-cations in zeolites results in strong local electric fields which can promote chemical transformations, for example photochemical oxidations of hydrocarbons (hc) with molecular oxygen, using light of longer wavelengths than would be the case in solution, since the surface electric-field is able to stabilise the necessary, initial collisional ($hc^{+\cdot}O_2^{-\cdot}$) charge-transfer complexes, rendering their formation thus accessible at lower energies. For example, the C–T complex formed by photoexcitation of tetramethylethylene (2,3-dimethylbut-2-ene) in zeolites X and L is stabilised to the tune of 3.5 eV, causing the absorption wavelength to tail into the visible region of the electromagnetic spectrum at 350 nm[42].

5. Free radicals produced by mechanical action

It is well known that the influence of mechanical stress on materials can cause the fracture of chemical bonds, or the transfer of electrons between donor-acceptor molecules, such that free radicals are formed. A good example of this is the detection of free-radical signals from samples of bone following milling or grinding[43].

The effect of mechanical action on synthetic polymers, and even on quite low molecular weight compounds, is also known to produce radicals. Such mechanical stress may come from milling, the action of pressure, compression combined with shearing deformation or shock waves, from explosives. As a potential practical application, the mechanical degradation of 1,2,3-trichlorobenzene, monochlorobiphenyl and other compounds was undertaken using a ball-mill with inorganic materials such as CaO added. On prolonged grinding, a degree of dechlorination close to 100% was achieved during a process that involved the formation of free radicals according to ESR measurements and yielded inorganic chloride anions[44]. Thus mineralisation of such materials might be achieved in this way. The types of compound which have been investigated include compounds with a weak covalent bond, donor-acceptor mixtures, energetic organic compounds (explosives), *etc*. Collectively, this field of chemistry has been termed ''mechanochemistry'', meaning the investigation of the influence of mechanical energy on the chemical (molecular) properties of materials. Some of these topics are now outlined.

5.1 *Mechanical decomposition of compounds with a weak covalent bond*

There are compounds (mainly dimers of very stable free radicals) which contain exceptionally weak bonds. The dimer of the archetypal free radical, triphenylmethyl (''trityl'') has a bond dissociation energy[45] of *ca* 45 kJ/mol, sufficiently low that it exists in equilibrium, in solution, with the free radical[46]. Other compounds have stronger, but still weak bonds, for instance alkylindanedione dimer, in which the interconnecting bond has a dissociation energy of 72 kJ mol^{-1} [47]. This is far smaller than the typical bond energies for organic compounds; for comparison, the dissociation energy for the central C—C bond in n-butane is *ca* 340 mol^{-1} [45]. Other compounds which demonstrate this feature are bis(2,4,5-triphenylimidazolyl)[48], 3,3′-bis(3-aryl-2-benzofuranosyl)[48], 2,2′-bis(2,3,4-triarylchromenyl)[48] and 2,2′-bis(2-aryl-3-benzothiophenolyl)[49]; all of which are susceptible to pressure, combined with a shearing deformation of the solid, which results in the formation of the respective (monomer) free radicals. Pressure alone does not have the same effect, since the shearing force is required to literally tear the two halves of the dimer apart.

Suitable apparatus permits the sample to be subjected to pressure within the cavity of the ESR spectrometer. During my time in the Chemistry Departments at Queen Mary and Westfield College, London University, I was given a Varian E9 ESR spectrometer by the Materials Department, which had been purchased with the intention of subjecting strands of polymers to mechanical stress in an attempt to correlate the free radical concentration resulting from ''snapped'' main–Chain chemical bonds with the mechanical load imposed. Apparently it worked well, but the project was abandoned when complex hyperfine structure emerged in some samples, rather than a single line with which to measure the unpaired electron concentration. The spectrometer is long gone, but I will be ever grateful both for this quirk of fate and to Dr Peter Reid for the machine itself.

ESR signals were detected in samples of Baltic amber (a resin), whose intensity was increased by milling with anthracene, acridine or calophony[50]. Immediately following the milling procedure, the intensity of the ESR signal increases about six times, but then decays once the mechanical process is terminated, and may be restored by further milling[50]. Indicators like phenolphthalein are also susceptible to this kind of mechanical stress, which induces both ESR signals and colour changes. The explosives, 1,3,5-trinitro-

1,3,5-triazacyclohexane (RDX) and pentaerythritol tetranitrate, provide an ESR spectrum of $\cdot NO_2$ on milling at 77 K[51].

5.2 *Formation of radicals by the action of shock-waves from explosives*

Another route, by which radicals are generated in solids by mechanical force, is through shock-waves, generated by explosions[52]. The mechanical energy is sufficiently great that even strong covalent bonds may be cleaved. It is believed that an initial decay of individual molecules takes place, releasing energy which sets-off secondary decays of other molecules. When the rate of localised heat generation (''hot spots'') exceeds the rate of heat loss, the explosion itself occurs, and radicals are produced by the rapid-heating of molecules. The ESR spectrum of $\cdot NO_2$ is detected following explosions of various materials, including RDX and ammonium nitrate[52]. Radicals are also detected in non-explosive materials, which have been subjected to shock-waves from explosives present in intimate mixtures with them.

5.3 *Radical-pair generation by mechanical stress on a donor-acceptor pair*

So far, we have considered radicals that are generally formed by cleavage of a weak covalent bond. One further possibility is that radicals may arise from the interactions between an electron donor and an electron acceptor. There are, in fact, numerous compounds known to behave in this way, under conditions of mechanical stress, giving rise to radical pairs[53]. If the two radicals are close enough that the unpaired electron from each may interact with the other, then the ESR spectrum takes on the particular form of a ''triplet-state''. The spectrum is characterised by the parameters $D_{\|}$ and $D_{\perp}$: in practical terms, $D_{\|}$ provides an indication of the distance between the two unpaired electrons, while $D_{\perp}$ measures the symmetry of their interaction. In some cases, the ''radical pair'' may withstand extraction into a solvent, and so is a ''biradical'' product of chemical bond formation between donor and acceptor, otherwise, the ''pair'' will be put asunder by the action of the solvent[54]. The simple action of grinding the materials together in a mortar for some minutes is all that is required to produce a detectable ESR spectrum.

6. Measurement of peroxyl radicals and nitrate radicals in air

Organic peroxyl radicals ($RO_2\cdot$) are the main chain-carriers in the atmospheric oxidation of hydrocarbons. They are formed during the daytime by reactions between $\cdot OH$ radicals and hydrocarbons and CO, and at night by reactions between hydrocarbons and ''nitrate'' radicals ($\cdot NO_3$), and from reactions of the Criegee intermediate produced by the interaction between alkenes and ozone. The night-time chemistry of $\cdot NO_3$ is as follows: $\cdot NO_3$ radicals are produced by the reaction between ozone and $\cdot NO_2$, then a rapid equilibrium is established between $\cdot NO_3$, $\cdot NO_2$ and N_2O_5. Both $\cdot NO_3$ and N_2O_5 can be removed by reaction with *hydrometeors* (literally, falling objects composed of water; *precipitation* consists of a stream of hydrometeors, in the form of droplets or ice crystals). This leads to the formation of dissolved $\cdot NO_3$, a process which provides a night-time sink for atmospheric NO_x. In addition, $\cdot NO_3$ radicals undergo addition reactions with alkenes present in the atmosphere, followed by addition of oxygen, to form β-nitratoalkylperoxyl radicals ($O_2NO-CR_2-CR_2-OO\cdot$). $\cdot NO_3$ also reacts with aldehydes to yield $RO_2\cdot$ radicals and nitric acid, while reactions of $RO_2\cdot$ with $\cdot NO_3$ lead to the formation of alkoxy ($RO\cdot$) radicals [equation (1)]. Hence, the $*NO_3$ radical can play a similar role as does NO during daytime[55], namely by initiating chain reactions that lead to the formation of $HO_2\cdot$ and $\cdot OH$ radicals at night [equations (2) and (3)]. In equation (2), the radical $RO\cdot$ is in fact one of type $RCH_2-O\cdot$ which transfers a hydrogen atom to O_2, forming $HO_2\cdot$:

$$RO_2\cdot + \cdot NO_3 \rightarrow RO\cdot + \cdot NO_2 + O_2 \quad (1)$$

$$RO\cdot + O_2 \rightarrow RCHO + HO_2\cdot \quad (2)$$

$$HO_2\cdot + \cdot NO_3 \rightarrow \cdot OH + \cdot NO_2 + O_2 \quad (3)$$

Measurements of these radicals have been made in the troposphere by sampling air at the top of a mountain (Schauinsland a mountain in Southern Germany with an elevation of 1,284 m) using a matrix-isolation apparatus[56]. The radicals were trapped from 8 L of air, with an efficiency of $>95\%$, in a D_2O matrix at 77 K over a period of 30 minutes. The samples were then transported, frozen in liquid nitrogen, to a laboratory at ground level for ESR measurements. The ESR spectra were analysed using a numerical procedure which fits the individual spectra of each radical component, and provides a

measure of their concentrations: the detection limit is 5 parts-per-trillion-by-volume (pptv) for $HO_2\cdot$, $RO_2\cdot$ and $\cdot NO_2$, and 3 pptv for $\cdot NO_3$ due to its narrower ESR linewidth. From a typical ESR spectrum, recorded from one experiment, the uppermost trace (A) is the original spectrum, and is dominated by $\cdot NO_2$, at a concentration of 0.65 parts-per-billion-by-volume (ppbv); subtraction of the $\cdot NO_2$ signal (B) yields the residual signal (C), which matches closely the structure of the $\cdot NO_3$ reference spectrum (D): a simultaneous fit of the reference spectra of $\cdot NO_3$, $HO_2\cdot$ and various peroxyl radicals yielded a concentration of $\cdot NO_3$ at 9.5 pptv, whereas the total amount of peroxyl radicals was less than 1 pptv.

The $\cdot NO_3$ levels were always found to be quite low, < 10 pptv. The concentrations of peroxyl radicals varied between almost 40 pptv and values below the detection limit of 5 pptv. The $HO_2\cdot$ concentration was mainly also at or below the 5 pptv detection limit[56]. The ESR method is, of course, specific for free radicals, and can form part of an overall sampling strategy in which other analytical methods are employed to analyse hydrocarbon and other trace gas components from the atmosphere, to provide an overall view and a test of atmospheric chemical kinetic models[55].

7. Determination of polycyclic aromatic hydrocarbons (PAHs) using ESR

Polycyclic aromatic hydrocarbons (PAHs) are probably the most widespread of all potentially carcinogenic and mutagenic chemical pollutants in the environment, and so the determination of PAHs is of vital importance in environmental monitoring[55]. They are produced in virtually all combustion processes and are generally present in environmental samples as very complex mixtures. Since the molecules of PAHs are diamagnetic, ESR does not immediately come to mind as the most obvious means for their identification and quantification; however, PAHs are quite readily oxidised to their corresponding radical cations, using a silica-alumina catalyst[57], of the kind used in the petrochemical industry for hydrocarbon ''cracking''. The catalyst is in an amorphous form, rather than being of the zeolite type, which can also produce radical cations from molecules with a sufficiently low ionisation potential. This has the advantage that larger PAH molecules can access the catalytic sites, whereas they would be excluded from the pores of a zeolite, zeolite Y does not admit molecules of anthracene or larger[58]. The resulting radical cation species are stable in the sorbed state on the

catalyst surface, and the conversion is quantitative. The catalyst is first heated in air at 800°C for at least two hours in a muffle furnace, and then is allowed to cool, under vacuum, to room temperature. The PAH solution, in toluene, is introduced to a sample tube, to which the catalyst is then added.

When known concentrations of perylene, anthracene, chrysene, pyrene and 3,4-benzopyrene were added sequentially, firstly in the range up to 0.5 nmol, then from 1 to 5 nmol, a straight line plot is observed of ESR signal intensity *vs* concentration. This indicates that the method is valid for the estimation of PAHs generally, and as present in mixtures, the experiment is measuring the total number of PAH molecules present, irrespective of their precise nature. In order to measure an overall signal intensity in mixtures of PAHs, it is necessary to over-modulate the spectrum: this has the effect of broadening the spectral lines so that all PAH radical cations are revealed in one single first derivative signal, whose peak-to-peak intensity may be taken as a measure of radical concentration[57].

7.1 Measurement of soot and PAH in urban air

The procedure has been applied to the analysis of the air in Sofia, Bulgaria[59]. Aerosols containing both mineral dust and soot with adsorbed PAH were collected by drawing 5 m^3 of air through a Whatman No. 1 filter paper. It is important to introduce some terminology here: PAH is often referred to by environmental workers as ''organic carbon'' (OC), while soot is called ''elemental carbon'' (EC); EC refers to the hard carbon-rich material on which OC is adsorbed, and both are produced together by combustion processes, as in incinerators, vehicle engines, and indoors by smoking and burning fuels. Three to five samples were collected at each of four locations: (1) by the side of a motorway, (2) 100 m away from the motorway (urban air), (3) in an office (where smoking is forbidden), (4) in a cafeteria (where smoking is allowed). The soot collected on the filters was measured directly by ESR, since it contains unpaired electrons (at this point, the PAH, OC is invisible). For the evaluation of the PAH, the filter was extracted with 10 mL of toluene, and 0.3 mL of the resulting solution was transferred to an ESR sample tube with a cracking catalyst introduced, in the form of a pellet. After one hour, the ESR signal from the total PAH radical cations was recorded, thus providing a measure of the OC content of the soot: both EC and OC concentrations were calibrated against a standard sample containing known quantities of a carbon–Char, prepared by

pyrolysing sucrose at 550°C. To ensure reproducibility in the relative peak-to-peak signal intensities and line-widths, the spectra were recorded simultaneously with that from a reference standard containing Mn^{2+} ions. It was found that the EC content decreased in the order: motorway > urban air > cafeteria > office, with values of 91.1 μg m^{-3}, 49.5 μg m^{-3}, 18.7 μg m^{-3} and 7.8 μg m^{-3}. However, the OC content (from PAHs) had values of cafeteria (76.6 μg m^{-3}), motorway (78.1 μg m^{-3}), urban air (32.5 μg m^{-3}), and office (2.7 μg m^{-3}). It is reasonable that the EC levels indoors are less than those outside, and are greatest on the motorway; the high level of OC in the cafeteria is probably caused by smoking, while that on the motorway must arise from exhausts.

The method has the advantage of simplicity over other, rather complex, procedures that are employed in the analysis of EC and OC. For example, these components may be determined separately using a thermal treatment to drive-off the volatile OC, followed by catalytic oxidation to form CO_2, which, after reduction to CH_4, may be quantified by various methods of gas-analysis. The temperature is increased up to 600°C at which the OC (principally PAH) becomes volatile and is removed in a stream of helium prior to their oxidation. The next step involves the removal of carbon particulate (EC) remaining on the filter, which is then also converted to CO_2 in an O_2-He stream[59]. ESR has been similarly employed in the analysis of diesel exhaust particles (DEP), taken at various points in the exhaust-pipe of a diesel engine, at the dust sampler of a highway tunnel (standard DEP), on the soundproofing wall alongside a heavy traffic road and on the filters. A very broad signal was detected from iron oxides and a second much sharper signal from carbon radicals. On annealing the DEP sample at 250°C, a dramatic increase was observed in the intensity of the latter signal, which suggests that a thermally activated carbonization of residual organics had occurred[60]. An investigation was made of summertime carbonanceous aerosols collected from the marine boundary layer of the Arctic Ocean, in which the relative concentration of what is described as black carbon (BC)–which is the same as EC in the Sofia study–was determined using ESR. It was found that the spatial distribution of BC from ship emissions was concentrated around the periphery of the Arctic Ocean, which suggests relatively intensive contamination by ships in the Russian and Canadian Arctic. As determined by gas chromatography-mass spectrometry (GC-MS)–rather than by ESR, as in the Sofia study–the abundance of PAHs on the BC

particles was determined in the range $142-2672\,\mathrm{pg\ m^{-3}}$ ($\mathrm{mean} = 702\,\mathrm{pg\ m^{-3}}$), which is much greater than previously determined using land-based observation, and hence ships appear to be a major contributor to PAH concentrations, certainly at some regions of the Arctic Ocean during the summer months[61]. It is thought that such carbon-contamination from shipping may contribute to the melting of the Arctic ice, potentially urging environmental consequences. If the Arctic continues to warm at its current rate a further decline in the amount of Arctic summer sea ice is expected. The consequences are that the global sea level will rise, with less habitats for polar bears but additionally an increased level of ship traffic which may further accelerate climate change.

8. ESR studies of soils and environmental biogenic substances

Soil is a complex material. It is heterogeneous, consisting of both organic and mineral components. The organic fraction is usually termed humus, and is composed predominantly of two types of material, humic substances and polysaccharides, which may constitute up to 80% of the total extractable matter in soil. Humic materials contain free radicals, which are of the semiquinone type, and are a mixture of ''transient'' species (with lifetimes of several hours), and others which are stabilised within the complex chemical structure of the material matrix. It is thought that the latter participate in the soil chemistry by acting as electron donors and acceptors[62]. Natural Fe^{3+}-fulvic acid complexes have also been characterised in some extracts. It has been shown that all 3d-transition metals form ''inner-sphere'' complexes with humic acids: Mn^{2+} ions are coordinated to raw peat or to peat humic acids octahedrally, whereas Cu^{2+} ions occur in square-planar arrangements with two carboxylate and two aliphatic nitrogen-functional ligands. It is reported that $VO_2{}^{+}$ ions occur in a square-pyramidal structure with four oxygen-containing ligands. In acidic solutions, diamagnetic Mn(VII), Cr(VI), Mo(VI) and V(V) oxoanions are *reduced* by humic acid to paramagnetic Mn(II), Cr(III), Mo(V), and V(IV) ions, but Cu(I) is instead *oxidised* to paramagnetic Cu(II)[63]. According to Cheshire *et al.*[64] copper is present in soil humic acid partly as a copper-porphyrin type complex, but in fulvic acid it occurs in some other complexed form. $VO_2{}^{+}$ ions form more covalently bonded complexes in fulvic acid than is the case in humic acid. In contrast, Mn^{2+}

Figure 4 *Organic cultivation of mixed vegetables in Capay, California. Note the hedgerow in the background. The latter is significant in permaculture/regenerative agriculture, or farming with low inputs of energy and artificial fertilisers and freshwater. It is thought that no-till farming practices applied across all the world's 14 million square kilometres of arable land might sequester 40% of anthropogenic (human-created) carbon emissions*[67]*. Credit: Hajhouse. http://upload.wikimedia.org/wikipedia/commons/3/38/Organic-vegetable-cultivation.jpeg*

complexes of both humic and fulvic acids are highly ionic in their bonding. In another study, Boyd *et al.*[65] investigated the mechanism of Cu(I) binding by sewage sludge humic acid, and concluded that Cu(II) forms two equatorial bonds with oxygen donor atoms originating from functional groups of the humic acid. The ESR data also indicate that the two Cu(II)-humic acid oxygen bonds occupy *cis*-positions in the square-plane of Cu(II), a result that is consistent with the formation of a Cu–Chelate. DFT calculations have been used to calculate pK_a values and g-tensor components for semiquinone radicals as a mimick for the kind of radicals present in humic acids. The results accord with the notion that naturally occurring stable semiquinone radicals (native form) are trapped in the humic acid macromolecule matrices which precludes their direct involvement in the acid-base equilibrium with short-lived radicals (transient form). The differences calculated for g-values for protonated and deprotonated model radicals are similar to those observed for humic acids, which permits an

identification of the stable radicals to protonated semiquinones, and the short-lived radicals to deprotonated radicals[66].

Jezierski *et al*.[67] have made a quantitative ESR study of radicals stabilised in the polyphenolic matrices of various biogenic materials: lichens, mosses, composts, soils, peats, brown coals and sewage sludge sediments. Both the raw materials and extracted fractions of humic acids were investigated. It was found that the g-value may be used as an indicator of the extent of transformation of organic matter. Composting of municipal solid wastes results in an increase of the g-value as the process proceeds. When the stage of compost maturity has been reached, the g-value changes become insignificant. For lichens, mosses, sewage sludge sediments, soil, peat and brown coals, the g-value is an important parameter, which correlates with the redox properties of the environment and the chemical composition of the material. For brown coal, the g-value decreases during coalification and correlates with humic acid content; carbonization of the coal also results in the same trend in the g-value. Treatment of these materials with ammonia gas also causes an elevation of the g-value, which is greatest for lignites. Changes in the spin-concentrations are found to occur as a result of quite different phenomena: in lichens, there is an increase in the spin-concentration in response to air-pollution; in degraded soil, the spin-concentration increases with its organic carbon content; in lignites the spin-concentration increases with the humic acid content. It was also found that the interaction of humic substances with metal ions also alters the spin-concentration: in the interaction of peat humic acid and lignite humic acids (both raw and carbonized), both with VO^{2+}, complex variations in the spin-concentrations are found, which depend on the ion concentration and on other conditions of sample pre-treatment such as temperature[67]. Changes in soil organic matter (SOM) fractions under no-till cropping systems have been investigated using ESR[68]. Though the topic is controversial, it is claimed that up to 40% of the CO_2 emitted by human activites (26 billion tonnes/year) could be sequestered in the form of soil SOM[69] if no-till/regenerative farming practices (Figure 4) were employed rather than intensively fertilised tillage as in modern industrialised agriculture which breaks-down soil and causes a substantial loss of its carbon content in the form of greenhouse gases. The energy-inputs might also be reduced to one-quarter for regenerative no-till farming, of those required for fertilised tilled crop production[69]. On the basis of a negative relationship between decay rates of SOM and the concentration of iron oxides, it was concluded that the SOM was

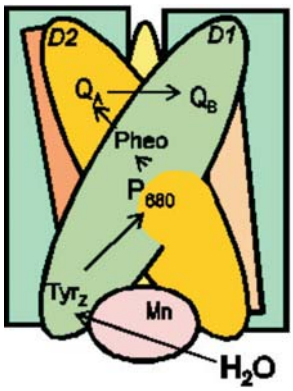

Figure 5 *The catalytic cleaving of water occurs at a manganese-containing cluster bound to the lumenal side of D1/D2, resulting in electrons which are transferred to P680* via *Tyr_z, a redox-active residue on D1. Electrons are transported from P680 to a mobile pool of plastoquinone molecules by subsequent redox reactions via Pheo, Q_A and Q_B. Reproduced with permission.*
http://www.photobiology.com/v1/hideg/ps2.jpg

physically stabilised by interactions with variable charge materials. This was confirmed by power-saturation curves measured by ESR for $20-53$, $2-20$ and $<2\,\mu m$ grain size fractions, in which saturation occurred less readily as the grain size decreased, indicating stronger interactions between semiquinone radicals and mineral components, as confirmed by higher concentrations of iron-oxides and kaolinite in the smaller particles[68]. The bioavailability of xenobiotics in soils and sediments depends on a number of interlocking factors. In order to obtain direct information on the molecular level as to the environment of xenobiotics in natural porous media, an ESR study was conducted using Tempol and Tempamine$^+$ as spin-probes. In batch experiments with Ca-hectorite suspensions and pastes, it proved possible to distinguish between probe molecules in different locations: adsorbed, in bulk solution or in large interstitial pores. The spin-probe underwent degradation in the bulk solution and the kinetics for the release of the probe molecules from the clay aggregates and/or paste could be monitored, but in any case the process was complete in under a day, indicating that the probes are only weakly contained by the hectorite. Further potential applications of this technique in soil science are considered[70]. It is, of course, the mobilisation of pollutants in soils, pesticides such as carbofuran[71] that permits their degradation (mineralisation) by microbial action and hence the ESR-based method might cast some light on the mechanisms by which this occurs.

ESR has also been applied to the determination of the effects of air-pollution on over 800 samples of lichens[72]. In a study of lichens from Lower Silesia (southwest Poland) a statistical correlation was found between the annual average atmospheric concentration of SO_2 and the concentration of semiquinone radicals in *Hypogymnia physodes* thalli. Similar results were obtained for *Umbilicaria* species from the Karkonosze Mountains. A plot of the distribution of the semiquinone radicals within the lichen thalli was also derived. Interestingly, the action of NO_2 on *Umbilicaria* species resulted in the production of iminoxyl radicals in the thalli. It was concluded that the increased production of semiquinone radicals in lichen thalli by atmospherically polluted environments and the degradation of lichen acids to β-diketones are probably parallel processes. The iminoxyl radicals derived from the β-diketones in the lichen matrix showed anisotropic ESR spectra at room temperature; and when extracted into a range of organic solvents, a linear correlation was found between the isotropic ^{14}N couplings and the Dimroth-Reichardt solvent polarity parameters (E_T).

9. Consecutive estimation of nitrite and nitrate ions in vegetables and fruits

Nitrite ions can be measured using ESR spectroscopy, based on their quantitative liberation of NO in an acidic solution of $FeSO_4$ [equation (4)]. NO is swept from the reaction vessel using a stream of air, and into a trap containing a 0.01 M solution of [Fe(*DETC*)$_3$], to form [Fe(NO)(*DETC*)$_2$], whose concentration may be measured using ESR. Both the production and trapping of NO are quantitative. The nitrite concentration having been so determined, it is possible to make a sequential and quantitative determination of nitrate, since, in the same acidic $FeSO_4$ solution, NO_3^- is converted to [Fe(NO)SO_4], according to equation (5), which remains in solution, during the nitrite measurement.

$$NO_2^- + nFeSO_4 + mH_2SO_4 \rightarrow NO + \ldots \quad (4)$$

$$NO_3^- + nFeSO_4 + mH_2SO_4 \rightarrow [Fe(NO)SO_4] + \ldots \quad (5)$$

On addition of sodium diethyldithiocarbamate to this solution, [Fe(NO)(*DETC*)$_2$] is formed, and may be extracted with a known volume of toluene, and its concentration determined by ESR. Full experimental details for this consecutive estimation of nitrate and nitrite in vegetables and fruits by ESR are described, based on the selective reactions of nitrate and nitrite ions to yield a stoichiometric

amount of the ESR-active mononitrosyldiethyldithiocarbamate complex of iron in aerobic conditions. Since, NO and NO_2 (which may be present in the air) give the same reaction, the detection limit depends on their background concentration in the air. The ESR response is found to be linear up to 2500 μg of NO_2^- and 16 000 μg of NO_3^-. The applicability of ESR spectrometry for estimation of both nitrate and nitrite content is demonstrated by the analysis of 18 vegetables and fruits, available in the local markets in Sofia (Bulgaria), grown with the use of mineral fertilisers. It is concluded that the amounts of both nitrite and of nitrate differ considerably from one species to another, and that both are far lower in home-grown produce than in fruit and vegetables bought in a local market[73].

10. Lipid Peroxidation by solid particles: silica, asbestos, coal-dust

There is current concern over the toxicity of various minerals, especially asbestos caused by their inhalation, leading to lung diseases, including specific types of cancer, although their precise mode of action remains uncertain. However, as shown in the examples below, there is evidence from spin-trapping studies that these materials can initiate free radical formation, and so might precipitate lipid peroxidation[1] of the pulmonary cell membranes[74]. In crocidolite asbestos[75], it is known that iron is present and that it can reduce O_2 and participate in Fenton-type reactions. Because of the importance of these reactions in crocidolite-induced toxicity, studies have been made, on three different types of crocidolite fibres, to determine the factors which control the activity of iron in catalysing the two reactions. Results show that the total concentration of iron in crocidolite fibres is not an appropriate parameter for characterising the activity of this mineral, which seems rather to be controlled by the valency and the location of the iron in the lattice, and also by its availability for mobilisation from these minerals.

Following this is a study of crocidolite which has been ''detoxified'' [76].The fibres were treated with ferric oxide salts to form a metal-micelle polymer surface coating which prevented physiological reactions with the mineral. This detoxified crocidolite was tested for its ability to produce $^{\cdot}OH$ radicals from H_2O_2. It was found that the intensity of the DMPO-OH radical adduct signal was indeed reduced from that obtained from the native crocidolite fibres. Similar experiments showed that the ability of the detoxified crocidolite to reduce oxygen was also decreased compared with

the native mineral. The availability of ferrous iron present in the two crocidolite fibres to catalyse the above reactions was investigated with the chelating agent ferrozine. The results indicate that ferrozine was able to remove fewer ferrous ions from detoxified crocidolite than the native form; moreover, Mossbauer spectroscopy shows that the detoxification process results in both bulk and surface changes in the co-ordination chemistry of the detoxified sample. The detoxification process also introduces a surface coating comprising ferric ions which shield near-surface ferrous ions and consequently reduces the Fenton-type reactivity of the fibres. On the subject of ''detoxification'' of crocidolite, the same group[77] report the treatment of crocidolite fibres with microwave radiation at different temperatures: this reduced the Fe^{2+}/Fe^{3+} ratio, according to Mossbauer measurements, and produced a concomitant decrease in the ability of the fibres to peroxidise linoleic acid.

At least one *in vivo* study has been made of the toxicity of asbestos, using a spin-trapping technique[78]. 180 day-old rats were instilled intratracheally with either 500 micrograms of crocidolite or saline; 24 hours later, histologic examination of the lungs revealed a neutrophilic inflammatory response. ESR examination of the chloroform extract from lungs exposed to asbestos showed a spectrum consistent with a carbon-centred radical adduct while those spectra from lungs instilled with saline revealed a far weaker spectrum. The adducts are nearly identical with ethyl and pentyl radical adducts, providing evidence of *in vivo* lipid peroxidation resulting from asbestos exposure[78]. The adsorption of neutral and charged nitroxides from their solutions onto asbestos fibres was investigated using ESR, some of which contained an hydrophobic chain attached to the nitroxide group while in others it was absent. The four different asbestos fibres studied were chrysotile (which belongs to the serpentine group), and anthophyllite, amosite, and crocidolite (all of which belong to the amphibole group). It was found that the ''chain-free'' nitroxides (Scheme 1) 4-hydroxy-TEMPO and $TEMPYO^{-}$, being neutral and negatively charged respectively, were barely adsorbed by the positively charged chrysotile surface ($<10\%$), while the positively charged nitroxide CAT1 (Scheme 1) was better adsorbed to the extent of 25% by the negatively charged anthophyllite fibres. As expected, a reduction in the rotational correlation time was observed by interection of the spin-probe with the asbestos surface. The presence of the hydrophobic chain attached to the nitroxide group encouraged the formation of surface aggregates and led to a string enhancement of surface adsorption. The doxylstearic acids were preferentially adsorbed by chrysotile to

the extent of 80% an effect that was enhanced as the solvent polarity increased and as the chain length between the carboxylic and the doxyl groups increased. The positively charged surfactants (Scheme 1) CAT10 and CAT16 were adsorbed preferentially by anthophyllite fibres. Amosite fibres showed poor adsorption, whereas the ESR spectra from crocidolite samples were scarcely detectable, because of spin–spin interactions between the adsorbed radicals and paramagnetic surface metal ions. The close proximity of the surface adsorption sites favoured a high local concentration of radicals adsorbed on the chrysotile fibres, while in contrast low-packed surface aggregates were formed at the anthophyllite surface, since the interacting sites were rather more widely dispersed[79].

Another report shows that the $^{\cdot}OH$-generating potential of coal dust correlates positively with the surface iron content of the coal dust[80]. Two other papers describe results for the inhibition of quartz-induced lipid peroxidation. In one[81], an alkaloid used in China to treat the lesions of silicosis, is tested for its antioxidant activity: it is found that tetrandrine reacts efficiently with $^{\cdot}OH$ radicals generated by the reaction of freshly fractured quartz particles with an aqueous medium, and also scavenged $O_2^{-\cdot}$ radicals produced from xanthine/xanthine oxidase. A significant inhibition of linoleic acid peroxidation by freshly fractured quartz particles was also found. Taurine-based compounds were similarly investigated[82]: it was discovered that hypotaurine, but not taurine, caused a significant reduction in silica-induced peroxidation, again using linoleic acid as a model lipid.

11. Detection of reactive oxygen species in the photosynthetic apparatus of higher plants under light stress[83]

Plants which perform photosynthesis using oxygen have developed a balanced system of defence against reactive oxygen species (ROS) which involves both enzyme and non-enzyme mediated pathways. This is necessary, since such reactive species are produced in chloroplasts, under the influence of sunlight, to which the lipid components of their thylakoid membranes would be sensitive to attack. Under normal conditions, the system is efficient, and prevents significant damage, but under conditions of stress, as caused by both natural and artificial agents of pollution, the system may become overloaded, to the detriment of the plant. The principal activating factor is sunlight itself, since it can, under appropriate circumstances, activate oxygen into reactive forms.

When there is an excessive flux of solar radiation, such species can initiate the breakdown of membranes, proteins and pigments. Alternatively, damage may occur in consequence of a reduced efficiency in the capacity of the plant to utilise protons. The overall and complex interplay of these processes is called photoinhibition (PI) (which results in a decrease in photosynthetic activity), and photosystem (PS) II is thought to be the primary target of damage.

PS II is a pigment protein complex with a reaction centre that contains a heterodimer of two membrane spanning proteins, D1 and D2, which either bind or contain the redox cofactors involved in the central electron transport. The bound components are: the primary electron donating chlorophyll dimer (P680); the primary electron acceptor, pheophytin (Pheo); the secondary electron accepting quinones Q_A and Q_B. The catalytic cleaving of water occurs at a manganese-containing cluster bound to the lumenal side of D1/D2, resulting in electrons which are transferred to P680 *via* Tyr_z, a redox-active residue on D1. Electrons are transported from P680 to a mobile pool of plastoquinone molecules by subsequent redox reactions *via* Pheo, Q_A and Q_B (Figure 5).

Good model systems for studying light-induced stress in plants are: oxygen-evolving thylakoid membrane, PS II and other subthylakoid membrane preparations. Such *in vitro* studies have disclosed two main routes, which are dubbed ''acceptor site induced'' and ''donor site induced'' photoinhibition (API and DPI, respectively). Both API and DPI cause the impairment of PS II electron transport, followed by the specific degradation mainly of the D1 reaction centre protein and, to a lesser extent, of the D2 protein; while the result of more protracted PI is more general membrane damage – as signified by the detection of lipid peroxidation products. The two forms of PI are distinguished on the basis of differences in the primary site of electron transport malfunctioning, fragmentation pattern of the subsequent D1 protein degradation, as well as in the light intensity and oxygen requirement of the two processes. A third, alternative pathway of PI has been preposed to occur under conditions of low light intensities. ROS are also likely involved in this process, but their predicted yield lies below the limits of detection for the methods normally used to investigate them. Both models of PI assume the formation of active oxygen (Figure 6). In API, singlet oxygen production is believed to be caused by increased formation of a triplet state of chlorophyll in the reaction centre, and is a consequence of over-reduction of the first quinone electron acceptor in PS II. DPI occurs when electron flow

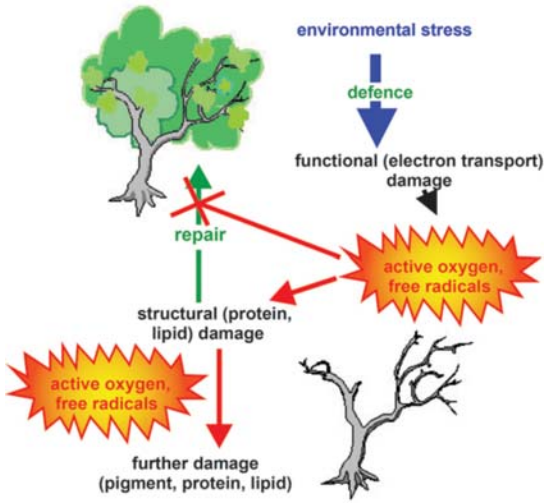

Figure 6 *Formation of "active oxygen" in plants during photosynthesis. Reproduced with permission. http://www.photobiology.com/v1/hideg/intro2.jpg*

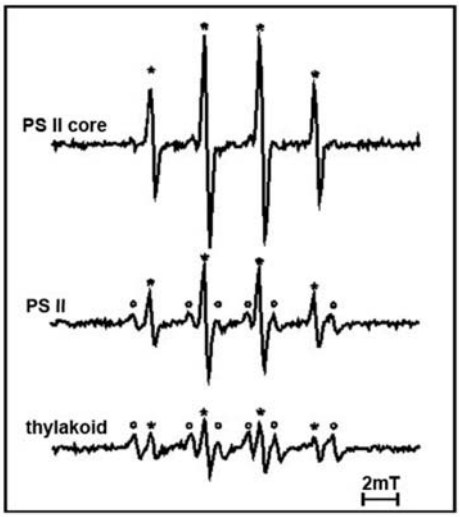

Figure 7 *ESR spectra recorded from a series of samples with increasing PS II purity (thylakoid membranes, PS II, PS II core complex preparations) which suggest that the primary event is* ·OH *radical production, which then causes the formation of other, carbon-centred radicals by damage to protein and polysaccharide components of the membrane. It is important to emphasise that these experiments were done under laboratory conditions, which provided a much stronger oxidative stress than would apply in the field situation.*
Reproduced with permission. http://www.photobiology.com/v1/hideg/uv_dmpo.jpg

from water to P680 is insufficient. There is consensus that the damage is triggered by the strong oxidants ($P680^+$ and Tyr_z^+) created by the primary charge separation and whose lifetime is prolonged in consequence of inoperative water splitting. In such case, both electron transport and protein damage proceed in the ansence of oxygen, even upon illumination with relatively lower intensities of PAR.

Similarly to PI caused by excessive PAR, UV-B (280–320 nm) irradiation causes a multitude of physiological and biochemical changes in plants, although these two types of light stress differ in a number of respects. Increased doses of UV-B radiation reaching the Earth's surface because of stratospheric ozone depletion have encouraged investigations into this form of light stress. It is well known that UV-B radiation causes the rapid inactivation of photosynthetic electron transport, altered pigment composition, loss of membrane integrity, and that it may result in the dimerisation of thymine bases and lesions in DNA. The increased synthesis of flavinoids, which are very efficient quenchers of ROS, as well as the increased expression of genes for flavinoid biosynthesis imply the involvement of ROS in the process. In the thylakoid membrane, the primary target for UV-B is PS (II); damage by UV-B involves functional impairment of PS II electron transport and degradation of PS II reaction centre proteins, primarily D1 and D2.

11.1 In vitro *studies.*

In vitro, it is found that the production of singlet oxygen is a unique characteristic of API, among the three forms of light-stress, and it does indeed arise in PS II. Singlet oxygen may trigger the subsequent D1 protein damage either directly or by causing a specific change in conformation which renders the protein susceptible to proteolytic damage. In addition to the role of this reactive but non-free radical oxygen species in API, the involvement of oxygen free radicals is quite possible, considering the proposed molecular mechanisms of both API and DPI. Indeed, the formation of radicals is evidenced by the reduced photoinhibition caused when radical scavengers or antioxidant enzymes such as superoxide dismutase (SOD) are introduced. PI induced free radical formation has been supported by spectrophotometric measurements in non-oxygen-evolving PS II preparations, and also directly, using ESR, in thylakoid membranes. In DPI, it is mainly $\cdot OH$ radicals and superoxide radical anions that are produced. It was found that free radical formation required the presence of oxygen during API

but not in DPI, demonstrating that the production of ROS and the propagation of PI are closely related. UV-B radiation also results in the production of free radicals but not of singlet oxygen, which demonstrates that the primary site of UV-B induced electron transport impairment is different from that of PI by excessive levels of PAR. In thylakoid membranes, UV-B radiation results in a parallel production of several different, mainly ·OH and carbon-centred, radicals. Comparing a series of samples (Figure 7) with increasing PS II purity (thylakoid membranes, PS II, PS II core complex preparations) suggests that the primary event is ·OH radical production, which leads-on to other radicals as products of its reactions with various components of the systems being investigated.

Superoxide radical anions are formed as by-products during the operation of photosynthetic electron transport. Their site of origin is PS I, where molecular oxygen provides an alternative sink for electrons in illuminated thylakoid membranes, when NADP is absent. Accordingly, superoxide radical anions can be trapped in isolated thylakoid membranes with Tiron (the disodium salt of 4,5-dihydroxy-1,3-benzenedisulfonic acid). The signal was inhibited by DCMU (which blocks the electron transport between PS II and PS I), increased by the addition of methylviologen, and no superoxide trapping was observed from the PS II core complex, even under conditions of API. These results demonstrate that the observed ESR signal does indeed arise from the trapping of superoxide from PS I by Tiron. In addition, API caused only a marginal increase in the ESR signal intensity from thylakoid membranes, indicating that superoxide is not the main promoter of API. In contrast, DPI resulted in a dramatic production of superoxide in PS II core complexes. Superoxide radical anions are also produced in thylakoid membranes and PS II preparations exposed to UV-B radiation; however, Tiron is itself slightly sensitive to UV-B which limits the precision of the conclusions which may be drawn.

ROS in vivo

While these *in vivo* experiments indicate that ROS are plausible candidates in the *in vivo* processes of light stress, such an actual investigation is tricky. Introduction of 2,2,5,5-tetramethylpyrrolidine into intact leaves indicates that singlet oxygen is being produced; however, it is found that the resulting nitroxide is rapidly metabolised in the leaf, which may make quantitative studies difficult. This difficulty in studying actual plant tissue is really the same as is

encountered in studying animal tissue, and it is plausible that the procedure of extraction of the hydroxylamine product of the nitroxide formed from 2,2,5,5-tetramethylpyrrolidine by oxidation by singlet oxygen, followed by re-oxidation to the nitroxide would prove fruitful. Spin-trapping studies of radicals in plant tissue is similarly difficult, since the almost ubiquitous presence of ascorbate and other reducing agents also reduces the resulting spin-adduct nitroxides, rendering them undetectable. Rapid post-stress isolation of thylakoid membranes with the spin-trap present can diminish this effect, as may be illustrated in the example of detecting free radicals in leaves that have been exposed to UV-B radiation. It is, however, important to bear in mind that the radicals detected may not be the primary species formed *in vivo*, but are products of such initial damage. Alternatively, the increased quantities of ascorbyl radical, formed from ascorbate, may provided a natural marker of stress in plants. It is hoped that the detection of singlet oxygen using 2,2,5,5-tetramethylpyrrolidine or Tiron, and of radicals with spin-trapping and the ''natural'' ascorbyl radical marker, may be used in the development of more rugged crop strains, able to resist an increasingly harsh environment.

12. Molecular mobility and intracellular glasses in seeds and pollen

Deterioration of seeds and pollen during storage involves many physical and chemical changes, including the disruption of the integrity of cells, decreased enzyme activities, lipid peroxidation, de-esterification and Maillard reactions[84,85]. Since it is known that glasses are formed in biological tissues during their dehydration, it has been proposed that their formation is a major factor in determining the rates of deterioration during storage[86,87]. It is thought that the presence of intracellular glasses decreases molecular mobility and impedes diffusion within the cytoplasm, thus slowing-down harmful reactions and changes in structure and chemical composition during ageing[88,89]. Using a spin-probe method, motional correlation times can be estimated[90] and correlated with bulk properties such as glass formation and storage stability.

In one study[91], mature male inflorescences of cattail (typha latifolia L.) were collected from fields near Wageningen, in The Netherlands, and allowed to shed their pollen in the lab. Pollen (94% germination) was exposed to a liquid germination medium containing 2.5 mM of the polar spin probe CP (3-carboxylproxyl).

There are a number of interesting details forthcoming from this investigation. In the first place, as measured at $-150°C$, when molecular motion occurring at a rate $>10^{-8}$ s is quenched, the separation between the extremum features of the CP spectrum ($2A_{zz}$) provides information about the polarity of the local environment of the spin-probe. In pea axes, the maximum $2A_{zz}$ was found to decrease with decreasing water content from 74 G to 70 G, whereas in cattail pollen, it changed accordingly from 72.5 G to 71.5 G. On increasing the temperature, the ESR spectra reflect the onset of molecular motion by an initially steady decrease in $2A_{zz}$, which at a particular point falls abruptly. It was found that with an increasing water content, the sharp decrease in $2A_{zz}$ began at lower temperatures, and at a loading of 0.16 g water/g it coincided with the melting point of ice, which indicates that bulk water is present in the pea axes cells. Similar results were found for pollen. Saturation-Transfer measurements (ST-ESR) were employed to gain a more detailed insight into the kind of molecular motion involved, by estimating values of τ_R for the CP probe molecules. In summary, it was found that during the drying of both cattail pollen and pea-axes, the τ_R for the spin-probe decreased from 10^{-11} s in the fully hydrated state to 10^{-2} s in the dry state[91]. This essential strategy was subsequently employed to demonstrate a likely correlation between molecular motion in the cytoplasm of lettuce seeds and storage lifetime, for which a ''viability equation'' was derived[92].

13. TEMPOL radicals in dry cotton

I have followed this project with some interest, since it was first initiated in my laboratory in Liverpool on a consultancy basis with Unilever Research[93], but via a brief consultation in Cardiff, later moved to the University of Stuttgart, along with its funding. The basis of the work is the adsorption of the spin probe, TEMPOL onto cotton, which is the world's most important clothing material. The absorptive properties of cotton are well known, when clothes are washed. This is due to the presence of amorphous regions where the pores of the material are located, and that the material is poly-saccharide in nature, so favouring hydrogen-bond formation with water molecules. Cotton[94] contains both regularly arranged crystal-lites, and irregular arrangements which provide the amorphous regions. The crystallites are roughly $10\,nm^3$ cubes, which are divided by amorphous areas, containing pores with a distribution in their average cross-sections ranging up to 3 nm. The amorphous regions are mainly responsible for the overall absorptive character

of cotton, since they provide 42% of the volume of the material, and are freely accessible to external molecules.

In a spin-probe study[95], 10 mm × 20 mm pieces of cotton were soaked in solutions of TEMPO dissolved in ethanol, in the concentration range, 6×10^{-5} to 5×10^{-2} M, then the residual solvent was evaporated. The probe was adsorbed in three main forms, in relative proportions that depended on concentration: (1) a mobile fraction, probably occupying the amorphous pores, in association with water; (2) a truly surface *adsorbed* immobilised fraction, adsorbed on the surface of the crystallites, (3) a bulk fraction (aggregate) of TEMPOL radicals which presents itself by a relatively broad single line. As the TEMPOL loading increases, the apparent viscosity in the pores also increases, and it is concluded that the TEMPOL molecules are deposited in pores of differing viscosity: those of lower viscosity are filled first, and then steadily pores of increasing viscosities, so that there is an apparent increase at higher loadings. When the TEMPOL loading is less than 3×10^{-3} mol kg^{-1}, the aggregated fraction is present in negligible quantities, such that an equilibrium can be considered between the mobile and adsorbed fractions only: mobile⇌adsorbed. The equilibrium, mobile⇌adsorbed, may be expressed by an equilibrium constant, K, from the temperature dependence of which, values for the molar enthalpy (ΔH^o) and entropy (ΔS^o) of the adsorption process were obtained by fitting the data to equation (6) [where R is the molar gas-constant (8.314 J mol^{-1} K^{-1}].

$$-\ln K(T) = -\Delta S^o/R + \Delta H^o/RT \tag{6}$$

It is a general feature of adsorption – literally on surfaces, which are in general, inhomogeneous, with sites that provide differential sorption energetics – that the derived values of enthalpy (ΔH^o) and entropy (ΔS^o) differ according to the degree of loading of a specified probe molecule. Thus, as TEMPOL is adsorbed onto cotton at the higher loading ($> 3 \times 10^{-4}$ mol kg^{-1}) the adsorption enthalpy is *ca* 50 kJ mol^{-1}, but increases up to *ca* 80 kJ mol^{-1} at the lowest loadings, which correspond to the viscosity changes already mentioned. Thus, the regions with lower viscosity and greater reorientational freedom also contain more strongly binding adsorption sites. The entropies of adsorption are surprisingly high, with values between *ca* 0.2 and 0.25 kJ mol^{-1} K^{-1}, and it is suggested that they reflect the loss of motional freedom of the polysaccharide chains as TEMPOL is adsorbed on the surface of the crystallites[95].

14. ESR characterisation of the surface of carbon black, used for chromatographic applications

Porous carbon occurs in many forms, and indeed can be fabricated for particular applications. As a bulk material of substantial porosity and high surface area, porous carbon is used in environmental remediation strategies, either in clean-up operations when contamination has already occurred, or preventatively, to minimise the release of pollutants into the environment. Of environmental significance too, is that carbon materials are used as ''packings'' for chromatographic columns, and these are employed ubiquitously to analyse the nature and extent of general environmental contamination by organic materials. We have seen numerous applications of nitroxyl radicals, in their role as stable ''organic''–free radical–probes. ''Inorganic chemistry'' also provides probes, in particular those based on Mn^{2+}, Cu^{2+}, V^{n+} and Mo^{n+}. The presence of Fe^{3+} is readily apparent in many samples–both of inorganic and biological origin–but the varied and subtle range of coordination geometries inherent to the nature of iron renders considerable complexity in many samples; nonetheless, a rough range of ''g-values'' serves to provide ''fingerprints'' of particular kinds of local environment, tetrahedral, octahedral, and their variants of lower symmetry.

ESR has been used to investigate the adsorption capability and the surface interacting ability towards Cu(II) solutions ($CuCl_2$, $Cu(NO_3)_2$, $CuSO_4$ in water or ethanol) of various carbon blacks such as are used in gas/liquid/solid chromatographic applications, both graphitized and ungraphitized, selected on the basis of the surface area, namely, Carbograph1 (area $= 100\,m^2\ g^{-1}$), Carbograph4 (area $= 210\,m^2\ g^{-1}$), and Carbograph5 (area $= 560\,m^2\ g^{-1}$), which were indicated as C1g, C4g, C5g (g = graphitized), and C1ng, C4ng, C5ng (ng = ungraphitized). The EPR analysis was supported by surface analysis, by which means the surface area, the pore volume and the porosity were determined, and by atomic absorption to obtain the amounts of adsorbed Cu(II). Graphitization was found to cause a decrease in surface area, but C1g, at low surface area, showed a unexpected increase of the adsorption ability which was explained by the generation of a new surface porosity closed by graphite layers. The carbon samples showed a broad unresolved EPR signal due to mobile unpaired electrons in the carbon matrix. Graphitized samples presented a narrower signal than ungraphitized samples, the width of which increased as the surface area increased (with the exception

of C5ng in consequence of the large surface area being subject to the action of oxidizing agents) and upon prolonged thermal treatment. The signal intensity of the paramagnetic carbon centres was found to decrease upon the adsorption of Cu(II). Computer simulation of the EPR spectra of the solids following Cu(II) adsorption provided structural information on the nature of the Cu-surface site complexes, in which the Cu^{2+} ions were coordinated with surface, mainly oxygenated, polar sites. The process of adsorption was found to depend on the nature of the different Cu(II) salts, in regard to the solubility of the salt and the interacting ability of the counter-anion. Ethanol solutions are more strongly adsorbed at the carbon surface than water solutions. Adsorption is favoured by ungraphitized carbons with respect to their graphitized counterparts due to both the higher surface area, and the higher hydrophilicity of the surface. In summary, these carbon powders, widely used for chromatographic applications, show an adsorption capability towards Cu(II) solutions that is higher than expected as a result both of a defined porosity, and the presence of polar groups which are not eliminated by chemical surface treatments[96].

15. ESR dating

The Earth's crust is sufficiently abundant in radioactive elements that, over time, radiation-damage is caused to the materials of which it is composed and to artefacts contained within it. Therefore, if the background radiation dose-rate is known and the total dose received by a sample can be measured, it is possible to estimate the age of the sample. Ionising radiation (γ-rays from radioactive isotopes of elements such as uranium, thorium and potassium) causes ''valence band'' electrons in an insulating material to be ejected from atoms, leaving positively charged holes, while some of the electrons are captured at trapping-sites which they may be thought to enter *via* the higher energy ''conduction band''; the majority of the ejected electrons simply re-combine with the positive holes (in radiation chemistry, it is frequently the energy released during such charge-neutralisation events which causes the formation of free radicals by breaking chemical bonds). The trapped electrons (and positive holes) may be detected directly by ESR[97–112]; alternatively, by subsequently heating the sample or by exposing it to light, they may be released back to the positive holes, leading to light emission (luminescence). The release of trapped electrons by heating is called thermoluminescence (TL) and by light, optically stimulated luminescence (OST). A major advantage of ESR is that it provides a

''fingerprint'' of the type of damage centres produced, and which may be identified as molecular (''Free Radical'') species, in addition to determining their concentration. In the archaeology literature, the defects are referred to indiscriminately as ''trapped electrons''[97–112]. ESR has the further advantage that it conveniently spans the time interval between the older limit of ^{14}C dating and the younger limit of K–Ar dating, a period of roughly $10^3 - 10^6$ years.

Estimates of the age of a sample are made from ESR measurements using equation (7), in which D_E is the ''accumulated dose'', the total radiation dose that the sample has received over the time it has existed for, and is determined by the ''additive dose method'' (next section). The dose-rate, D', is considerably more tricky to determine, since it requires a knowledge of the concentration of radioactive elements (mainly, U, Th and K) both within the sample and in its surroundings, and the effect of cosmic rays must also be considered. The rather demanding and exacting procedures necessary to ensure a reliable evaluation of the dose-rate have been described fully by Grun[98,99].

$$\text{Age} = (D_E)/(D') \tag{7}$$

15.1 The additive dose method

The procedure is based upon the manner in which the ESR signal from a sample at its ''natural intensity'' is enhanced by artificial irradiation with γ-rays from a ^{60}Co source. The fit of ESR intensity to radiation dose is called the ''dose response curve''. In the simplest case, this is actually a straight-line, but more complex functions are often required to get a good fit to the data. In any event, the curve is extrapolated to the point of ''zero'' ESR intensity, and the accumulated dose (D_E) (the dose which had created the initial ''natural'' signal) is determined as the point of intersection with the x-axis. Background radiation creates unpaired electrons which are responsible for the ESR signal, whose intensity grows with time[97–100].

15.2 Methods of ESR dating

15.2.1 Tooth enamel

In part, ESR has a niche in dating since it can access samples which are too old for radiocarbon dating, and do not contain the vital elements for such dating from the uranium series or from K/Ar ratios. Bones and teeth are found in a majority of archaeological

sites, and while some workers are of the opinion that bones cannot be dated reliably using ESR, it is agreed that tooth-enamel can be, and so might provide chronological data as a general device in archaeology[108,111,112]. Tooth enamel is formed from hydroxyapatite to the extent of $>96\%$, in which this mineral is in contact with more organically rich materials (dentine and cementum). A comparison was made[99] between the spectrum of natural tooth-enamel and one from the same material following γ-irradiation. There are essentially two signals: one at $g = 2.0018$ and another at $g = 1.9976$, both from $CO_2^{-\cdot}$ radicals in hydroxyapatite. The spectrum was recorded using a modulation amplitude of 5 G, which enhances the relatively broad signals from $CO_2^{-\cdot}$ radicals, and means that a smaller receiver gain is required to detect them. This has the effect of reducing the intensity of signals from organic radicals that are produced simultaneously by the radiation. This method is often useful in suppressing overlapping signals from organic radicals which might otherwise introduce errors into the dating procedure by distortion of signals, from $CO_2^{-\cdot}$ radicals, which are being used to gauge the ''additive dose''.

15.2.2 Dating of shells

Shells are found in relative abundance at many archaeological sites, and ESR dating has been applied particularly to coastal deposits. Attempts to date ostrich egg shells resulted in dramatic underestimates of their ages, in comparison with other methods (amino acid racemisation), which is thought to be the consequence of a low thermal stability of the ESR signals[99]. The spectra recorded from shells are, in fact, often fairly complex patterns arising from mixtures of radicals, and it is sometimes difficult to deduce reliable dose-response curves from them. The main problem appears to be that of ''where to measure'', since the radiation response which leads to different spectral features and from different radicals is not uniform, and it appears necessary to identify appropriate deconvolution procedures (to separate signals from different radicals) prior to the measurement of a signal intensity from a particular region of the experimental spectrum. However, since shells are the only datable material available in some deposits, and ESR determinations can be made on relatively small samples, systematic efforts to optimise the reproducibility and accuracy of such measurements should prove worthwhile.

15.3 Some examples

There are many examples, which are described along with the whole basis of ESR dating, in excellent reviews written by Grun[98] and by Ikeya[97], and some recent studies are now mentioned. As alluded to in the last section, there are efforts ongoing to improve the precision and accuracy of spectral measurements, involving ''fitting'' procedures[110], either using simulations with a theoretical (Gaussian or Lorentzian) line-shape, or an experimental spectrum; the latter, not unexpectedly, so far gives the better result, as demonstrated by fewer ''residuals'' (which are the components effectively ''left-over'' by the fitting procedure, and hence reflect the errors implicit to the fit).

Most ESR dating measurements in archaeology have been made on tooth-enamel, and procedures are described by Grun for the extraction of this component of teeth in order to minimise contamination (sorption), principally by uranium, along with necessary corrections for the influence of irradiation by more weakly penetrating β-rays (electrons formed by the decay of certain radioactive nuclei)[97], both of which would otherwise complicate, or introduce errors into, the calculation of the dose-rate.

Matters of reproducibilty and errors have received attention[109]. Some of the oldest tooth-enamel dated using ESR comes from a hominin tooth (*Australopithecus robustus*), for which a best estimate of 1630 ± 160 ka was made (Figure 8)[101], and a maximum age of around 2100 ka (over *two million* years old!), using a different model for the dose-rate. Interestingly, two teeth from a bovid (hollow-horned, ruminant animal) were dated as being in the range of 100–200 ka, despite previous estimates of between 1000 ka and 2000 ka[101]. A revision of the estimate of the age of tooth enamel samples taken from the sedimentary sequence at Border Cave (Australia) has been made on the basis of a detailed gamma-ray survey and newly calculated beta-ray attenuation. It is concluded that the total dose rate is between 0 and 30% smaller than previously estimated, and hence the samples are between 0 and 30% older[102]; the results are now in better agreement with those obtained from ^{14}C dating and amino-acid recaemisation measurements. It is further concluded that the sedimentation sequence began around 200 ka ago. A revision of the age of dental material from Neanderthal remains at 122 ± 16 ka was also reported[107]. Other notable results are that the oldest human remains in Australia have been established at Lake Mungo[103], with an antiquity of $62{,}000 \pm 6{,}000$ years, and it has been shown that

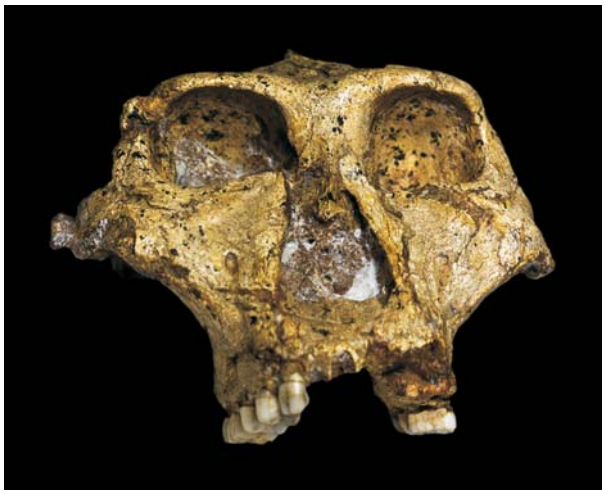

Figure 8 Paranthropus robustus *(considered for a time by the scientific community as* Australopithecus robustus*) is generally dated to have lived between 2.0 and 1.2 million years ago.* P. robustus *had large sagittal crests, jaws, jaw muscles, and post-canine teeth that were adapted to serve in the dry environment that they lived in. Credit: José Braga; Didier Descouens.*
http://upload.wikimedia.org/wikipedia/commons/a/a1/Original_of_Paranthropus_robustus_Fa-

Humans occupied Devil's Lair in Southwestern Australia as long as 50,000 years ago[104]. ESR can also be used to estimate the date of sea-level changes, from barnacles and corals. Barnacles live mainly in the intertidal zone and die when decreases in sea level changes cause them to be permanently exposed. Hence, if the barnacles can be dated, so therefore can past sea level changes, including those that occur because of ocean volume changes, crustal isostasy, and tectonics. Aragonitic mollusc shells can be dated by ESR from as young as 5 ka to ages of at least 500 ka. By chemically dissolving 20 μm from the shells, six barnacle samples from Norridgewock, Maine, and Khyex River, British Columbia, were tested for their suitability for ESR dating. It was found that the four Maine barnacle samples were not datable by ESR in consequence of interfering signals from Mn^{2+}. From two barnacles from BC, from which Mn^{2+} signals were absent, a mean ESR age of 15.1 ± 1.0 ka was determined, in good accord with dates obtained from ^{14}C-measurements of the barnacles themselves and of wood present in the overlying glaciomarine sediment. While stressing the need to ensure the stability of the ESR signals and to make a comparison with other barnacles of known age to validate the accuracy and reliability of the method, it would appear that ESR

can indeed date Balanus, and accordingly associated sea level changes[105]. While coupled $^{230}Th-^{234}U$-ESR measurements have become practically routine for dating teeth, this is not the case for dating corals. The age according to ESR depends on the time-averaged cosmic dose rate, $D_{cos(t)}$ (about which it is necessary to draw various assumptions), but the $^{230}Th/^{234}U$ determined date does not. Since the $D_{cos(t)}$ received by corals depends on attenuation of the radiation by all attenuating material, the $D_{cos(t)}$ response varies according to the depths of overlying water and of sediment cover. By combining the two methods, both the age and a unique $D_{cos(t)}$ can be simultaneously determined. $D_{cos(t)}$ can be predicted from the depth under water of a coral and its sedimentary history according to a given sea-level curve. Hence one can predict $D_{cos(t)}$ – if $D_{(cos,coupled)(t)}$ is in good agreement with $D_{(cos,sealevel)(t)}$ – which provides an independent validation for the curve used to construct $D_{(cos,sealevel)(t)}$. For six coral samples dated at 7 – 128 ka taken from Florida Platform reef crests, results were obtained that agreed well with previously determined sealevel curves. It is concluded that, where an entire reef can be sampled over a transect, a precise test for sealevel curves might be developed[106].

16. Measurement of the quality of tea-leaves using ESR

Tea is the most widely consumed beverage in the world, and it has been used as a daily drink and crude medicine in China and Japan for thousands of years. Green-tea, particularly, is considered to be an effective source of antioxidants, which are believed to be responsible for some of the positive health effects noted above. The main antioxidant components of green tea extracts include (+)-catechin, (+)-gallocatechin, (−)-epicatechin, (−)-epicatechin gallate and (−)-epigallocatechin gallate (EGCG).

The ESR spectra of tea leaves generally consist of two components: a single-line from semiquinone type radicals of 10 G width and a g-value close to free-spin (2.0023), resulting from oxidation of the plant material, and a broad component of >1000 G width and a g-factor of 2.025, from protein-bound Mn^{2+} ions[113]. The latter signal is interesting, since it provides a measure of protein degradation in the leaves: as the protein is degraded through oxidation, Mn^{2+} ions are released from the protein and are able to tumble freely, hence the resolution of six broad lines. It is notable that in cases where the protein degradation is greatest, the semi-

quinone signal is also at its most intense. In green tea leaves there is no indication of the six-line pattern, which is fully resolved in the spectrum of black tea leaves. The oxidation processes may be stimulated by irradiation with UV light, a procedure to which the different kinds of tea leaves respond differentially. For green tea leaves, the semiquinone radical signal increases slightly but steadily up to 8 hours of irradiation, while a more rapid increase is noted for black tea leaves. The results imply that the antioxidative potential of green leaves is about four times that of black leaves, in good accord with other studies which indicate a factor of six in the relative antioxidant effects of extracts of the two kinds of tea.

17. Green catalysts and catalytic media

The chemical industry faces unparalleled challenges, in terms of providing for growing markets and meeting the needs of a rising world population which aspires to a more advanced material quality of life, while minimising the environmental impacts of pollution from process–Chemistry. Nevertheless, the resources of this world are limited, particularly those of crude oil, and of the other fossil fuels, and hence an improvement in the efficiency of chemical manufacture is demanded, as met by higher product yields and selectivities, along with reduced energy costs. More effective catalysts and better reactor designs are key factors in realising these aims[114]. As noted previously, efficient photo-catalysts for the mineralisation of pollutants, in groundwaters, using visible-light are also highly desirable and are being sought. A review has been published entitled, ''Electron paramagnetic resonance: a powerful tool for monitoring working catalysts,'' the substance of which may be summarized thus: The method may be applied to the online monitoring of catalytic reactions on the basis of paramagnetic centres formed within the catalyst or free radicals formed as intermediates. EPR finds application for monitoring the synthesis and equilibration of solid catalysts and also their role in gas- and liquid-phase reactions, vanadia-containing oxides and FeMFI zeolites. The use of spin probes and spin traps for detecting hydrocarbon radicals in photocatalysis is illustrated. The potential advantage of making simultaneous EPR measurements with Raman and UV/vis is illustrated and discussion is given of limitations and future potential of the method in the field of catalysis[115]. Reactions of Al_2O_3-supported TEMPO with NO and H_2 and of SiO_2/Al_2O_3-supported $H_4PVMo_{11}O_{40}$ with methanol and formaldehyde were studied up to 400°C using a homemade heatable probe-head

equipped with a flow reactor. The TEMPO radicals were immobilised on the support in positions which impose a different reactivity to NO and H_2, as may be due to different accessibility, which changes during thermal treatment. Mo^{5+} is formed above 180°C, In addition to VO^{2+}, depending on the O_2 content of the feed, which is easily resolved Q-band but not at X-band[116]. Highly photoactive, tetrahedral Ti^{4+} sites can be created in mixed-phase TiO_2 nanocomposites, and which are shown to be an intermediate formed during the thermally driven phase-transformation from anatase to rutile[117]. Nitrogen-doped TiO_2 is a novel photocatalyst which can promote the decomposition of organic pollutants using visible light, and contains a number of different paramagnetic centres, such as NO and NO_2 radicals and other species, that interact strongly with the TiO_2 structure and are related to specific properties of the solid. In one paper, attention is focused on molecular species generated during the sol-gel synthesis process and segregated in cavities of the TiO_2 structure[118]. A review has been published of highly efficient titanium oxide-based photocatalysts with potential applications for the photo-degradation of organic pollutants, specifically methyl orange. Focus is given to the preparation and characterisation of TiO_2 photocatalysts prepared by transitional metal doping and noble metal deposition, and particularly a combination of the two methods. Fe^{3+} doped together with Au deposition on TiO_2 shows an excellent photocatalytic activity to degrade methyl orange (MO) under both UV and visible light illumination at wavelengths >420 nm. EPR demonstrates that Fe^{3+} substitutes for Ti^{4+} in the TiO_2 lattice, and XRD shows that Au exists as Au(0) on the catalyst surface. A mechanism is proposed to account for the synergistic influence of Fe^{3+} and Au in enhancing the photocatalytic activity of the catalyst[119]. Photoirradiation of TiO_2 nanoparticles by visible light in the presence of water-soluble, natural polysaccharide, arabinogalactan-complexes of β-carotene leads to a greater yield of the hydroxyl ($\cdot$OH) radicals than in the absence of the complex. Methyl and methoxyl radicals are formed when $\cdot$OH radicals react with DMSO and are trapped using PBN. Carotenoid-arabinogalactan complexes exhibit an enhanced quantum yield of free radicals and stability toward photodegradation over pure carotenoids, and the greater photocatalytic efficiency for carotenoid complexes is a consequence directly of the decrease in the rate constant for the back electron transfer to the carotenoid radical cation. Applications are stressed for TiO_2, in which these results might prove important, particularly in photodynamic therapy and in the design of artificial light-harvesting, photoredox, and

catalytic devices[120]. A multifrequency (9–95 GHz) EPR study has been reported for TiO_2 nanocrystals (NCs) capped by organic moieties prepared by both a nonhydrolytic and a hydrolytic procedure, respectively with a spherical or rodlike shape. The behaviour of the electrons promoted in the conduction band by UV irradiation and of the holes in the valence band has been monitored by means of EPR-detectable paramagnetic species so generated. The presence of paramagnetic species on the surfaces of TiO_2 NCs was used to account for the catalytic performance of these nanostructured materials which are highly catalytically efficient. An observed carbon-centred radical is proposed to be responsible for the higher catalytic activity of organic-capped nanosized catalysts, and indeed, by irradiation, the intensity of this signal with respect to the bulk Ti^{3+} signal is larger in the NCs prepared with a hydrolytic procedure, which are the more catalytically-active[121]. In the photooxidation of cyclohexane in mixtures with CH_2Cl_2 over TiO_2, singlet oxygen, $^1O_2$, formation was determined by the specific 2,2,6,6-tetramethyl-4-piperidone EPR assay. The yields of $^1O_2$ correlate with the amount of cyclohexanol detected in the mixtures, which provides convincing evidence that cyclohexanol is formed through the recombination of cyclohexylperoxyl radicals. Chloride yields were also determined and provide direct evidence for the active participation of dichloromethane in the photocatalytic system. A mechanism is proposed[122]. The role of dissolved oxygen in the photocatalytic degradation of phenol was investigated using polymer [poly-(fluorene-co-thiophene) with a thiophene content of 30% (dubbed PFT30)] sensitized TiO_2 (PFT30/TiO_2) with visible light irradiation. The photoluminescent (PL) quantum yield of PFT30/TiO_2 was about 30% that of PFT30/Al_2O_3, which shows that electron transfer occurs between the polymer and TiO_2. The virtually complete quenching of the reaction when the solution was saturated with N_2 shows the key role of O_2. When NaN_3 was present, which is an efficient quencher of singlet oxygen ($^1O_2$), a 40% reduction in the degree of degradation of phenol occurred. A roughly 60% decrease in the phenol photodegradation ratio was observed when alcohols were added to the medium, accounted for in terms of the scavenging of hydroxyl radicals ($\cdot OH$), the presence of which was confirmed by ESR/spin trapping, and that these are the major reactive species present in aqueous solution. In the absence of water, singlet oxygen ($^1O_2$) was the predominant species. It is clear that oxygen and reactive intermediates derived from it are critical in the photocatalytic degradation of phenol[123]. The encapsulation of

microperoxidases (NAPs) into molecular sieves of defined pore size, the mesoporous silica MCM-41 with 3 nm diameter channels, is a nanotechnological attempt to mimic the enzymatic activity of haemoproteins. Ferric microperoxidase-11 (MP-11) was entrapped in MCM-41, to provide a catalyst (Fe(III)MP11MCM41) with both the properties of catalase and monooxygenase. In a similar manner to catalase, Fe(III)MP11MCM41 was specific for hydrogen peroxide, leading to a high-valence oxidized intermediate, Compound II. In the presence of phenol (a reducing agent) a complete peroxidase cycle was confirmed by UV-visible spectrometry and EPR. Analysis of the reaction mixture by (HPLC/MS) showed that the product of phenol oxidation was 2,4-dihydroxyphenol, and hence in addition to catalase activity, the catalyst MP11 MCM41 also displayed monooxygenase properties. The latter feature is due to the fact that the MP-11 haem iron is able to promote homolytic cleavage of H_2O_2 with the generation of hydroxyl radicals[124].

These more fundamental principles have been applied to more pragmatic situations. For example, a traditional and popular lime tile using for decorating houses in Japan, ''Limix'', was coated with a titania sol and used to photochemically decompose formaldehyde, to address the problem of ''sick-building syndrome''. The photocatalytic activities of five types of lime tile material both with titania sol coating and without it were examined in a flow-type photoreactor based on the JIS (Japanese Industrial Standard). ESR was further employed to explore the potential photocatalytic mechanism in the coated tile. It was discovered that a higher efficiency was achieved when the lime tile was combined with a commercially available zeolite in comparison with the lime tile coated with an immobilised titania photocatalyst. The EPR spectrum indicates that oxygen-centred radicals and surface-trapped holes are formed in the titania sol, but this is entirely different from the spectrum observed in pure anatase and Degussa P25 titania, implying that the photocatalytic mechanisms are different[125]. A TiO_2-Ag doped slurry has been synthesized for concrete impregnation, to furnish a material with photocatalytic properties, for example of self-cleaning to prevent the build-up of organic debris on buildings. Ti and Ag centres were characterised by EPR, and also the activity of the material in generating $\cdot OH$ radicals in model situations[126]. The surface chemistry of activated carbons used as sorbents in a variety of applications has been studied using a combination of methods, including ESR[127]. An ESR-based characterisation of kaolin, used in large quantities in the paper industry as a filler

and coating material has been reported. For this application a high brightness grade of kaolin is required which depends greatly on its iron-mineral content, which can be assessed using ESR[128].

18. Fuel-related applications

The main waste material from biodiesel production is glycerol, raw fractions of which obtained from different kinds of transesterified oil, were investigated for their antioxidant and anticorrosive properties using respectively EPR and the Herbert method. It was found that those fractions rich in glycerol exhibited strong radical scavenging properties, in comparison with biodiesel and the pure oil. Interestingly, it was those fractions which displayed the greatest radical scavenging abilities that also showed the highest anticorrosive behaviour. It is proposed that the glycerol fractions may have applications as lubricants, hence the raw glycerol might be used in the absence of costly and lengthly purification procedures[129]. EPR spectra of crude petroleum contain an intense single line which is thought to arise from the superposition of signals from different radical species with very similar g-values, and moreover, the mobility of free radicals in crude oil is restricted by its high viscosity. Hence a low-viscosity oil was studied [marine diesel (bunker)] by X-band EPR spectroscopy in the temperature interval 170 to 400 K. Despite the viscosity at room temperature (2.5×10^{-3} kg m^{-1} s^{-1}) and the tumbling correlation time for free radicals of about 10^{-7} s suggesting a high mobility of free radicals in marine diesel, the EPR spectra still showed poor resolution up to 373 K. However, above 373 K, resolved lines were recorded: a superposition of a septet-quartet, a sextet-quartet and a quintet-quartet group of lines which were attributed to phenalenyl radicals and their derivatives. It is concluded that below 373 K, these radicals were present as diamagnetic dimers and hence undetectable to EPR[130]. In contrast with the isotropic X-band spectra, W-band spectra of diesel were found to show poorer signal-to-noise ratios and anisotropy in the A- and g- parameters[131]. EPR has also been used to characterise oil shale residue and rejects, calschist, shale file and retorted shale from the Irati formation in Brazil[132]. A study was reported of various fuel-samples made using ESR. As recorded at 298 K, spectra from heavy fuel samples proved to be characteristic of vanadyl porphyrins, along with a sharp intense signal close to $g = 2$ from organic radicals as are always present in asphaltenes. Two distinct spectral patterns were discerned among the gas-oil samples: the straight run gas-oil showed a single peak at $g = 2$,

while the light cycle oil spectra were characteristic of the phenalenyl radical. The pyrolysis fuels showed a single resonance from an organic radical and the mixed samples gave spectra similar to those of heavy fuels[133]. A study was made of the photochemical ''weathering'' of Brazilian petroleum from the Compos Basin, Rio de Janiro, as a film on seawater in relation to pollution by oil spills. The material displayed ESR signals from organic free radicals, vanadyl and iron(III) cations. After 100 hours of solar radiation exposure, the linewidth of the organic signal decreased by 10.6% and the g-value of the vanadyl signal was also decreased as a consequence of the degradation of porphyrin systems. It is concluded that solar radiation promotes the partial destruction of the asphaltene portion of the crude oil[134]. ESR has also been used to characterise radicals present in source rocks, by which means it has been shown that samples of kerogen collected at the shallow part of a petroleum deposit gave a broader peak than samples taken from deeper levels. Narrowing of the linewidth was caused by treatment of the sample with pridine but not by heating. A septet-quartet pattern is described which curiously is attributed to the tert-butyl radical, though it is quite obviously from phenalenyl radicals[135]. Samples of whole rock and isolated kerogen from three Alaskan North Slope wells were measured by ESR. Power-saturation studies of the single-line spectra showed a distinct correlation with the downhole maturation, the degree of aromaticity according to ^{13}C NMR, and with the beginning of the oil-window for the Kingak formation. Abrupt changes in ESR parameters indicate a change in the nature of the organic matter present and may reflect a facies (a body of rock with special characateristics) change[13].

18.1 ESR in fuel-cell research

While it is extremely debatable whether the putative ''hydrogen economy'' will ever become a reality, both on grounds of production[137] and storage[137,138] of hydrogen, and the shortage of platinum[137,138] to fabricate fuel cells (Figure 9) based on proton exchange membranes on a scale comparable with the 700 million vehicles on the roads worldwide, research continues into understanding the fundamentals of such devices, and an *in situ* study has been reported which used spin-traps to detect free radical intermediates in the H_2/O_2 catalytic cycle. Thus detected are hydroxyl radicals[138] at the cathode side of an intriguingly designed fuel cell[139,140] of appropriate dimension to fit within the resonant cavity of an ESR spectrometer. The issue of fuel cells is vexed, since there

is only sufficient platinum recovered annually that even if it were all used to make the so named proton exchange membrane (PEM) cells, which are those most suitable for use with hydrogen as a ''fuel'', if they are manufactured continually for the next 30 years, still only 7% of the world's present transportation fleet of 700 million vehicles can be so matched[141]. The major obstacles to such an entire transformation from an oil-based to a hydrogen-based transportation infrastructure are that firstly the hydrogen has to be ''made'' since it is not a fuel but an energy carrier. Most of the world's hydrogen is manufactured by catalytically steam-reforming natural gas[137,138], which results in an overall emission of CO_2, and thus a ''green'' source must be found, *e.g.* electrolysis of water using renewable electricity, *e.g.* from wind-power. The engineering feat required to inaugurate sufficient generating capacity by this means, however, is stupendous, and would take decades even were the manufacturing capacity for it already in existence. There is a further issue, namely of the availability of manufacturing raw materials, namely metals: as noted above, there is insufficient platinum available[141] to fabricate the PEM fuel-cells that would be required to ''burn'' enough hydrogen to propel more than a small fraction of the equivalent of 700 million vehicles as are currently on the world's highways, and indeed the currently vexed issue of rare earth (RE) metals, particularly neodymium needed for high-torque electric motors/dynamos, such as are used in wind-turbines, most of which are exported from China[142]. However, Chinese home-demand for REs is enormous given the thirst for all kinds of energy (including wind-power and other kinds of renewable energy) to underpin the relentless industrial growth of a nation that is predicted to overtake the United States as the world economic superpower by the end of this decade. In consequence, China has announced it will restrict its exports of REs onto the world markets, in order to meet its own agendas, which casts doubt on the growth of renewable energy in the world overall[142]. Hence, in the absence of alternative materials to replace platinum in this particular application, it is unlikely that transportation can be maintained at anywhere near current levels by means of PEM fuel cells, in addition to making enough hydrogen to run them on in the first place[141]. Nonetheless, fundamental studies continue in an effort to determine the durability of the PE-membrane itself under the harsh and aggressive working conditions of a working fuel cell. By introducing a spin-trap to a working fuel cell, specially designed to fit inside the cavity of an ESR spectrometer, one group has investigated a Nafion 115 membrane and another membrane free

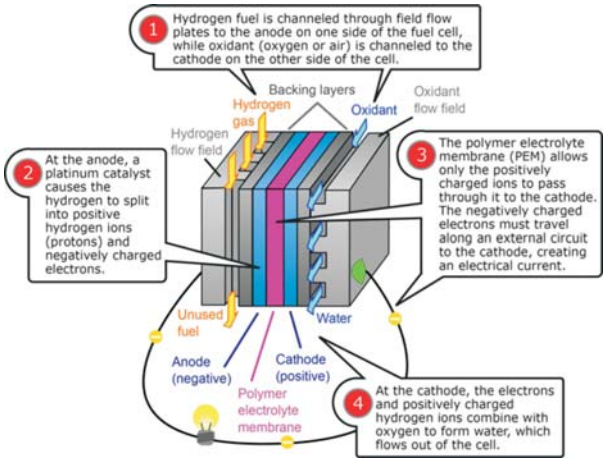

Figure 9 *Construction of a high temperature PEMFC: Bipolar plate as electrode with in-milled gas channel structure, fabricated from conductive plastics (enhanced with carbon nanotubes for more conductivity); Porous carbon papers; reactive layer, usually on the polymer membrane applied; polymer membrane.*
Credit: Jafet. http://upload.wikimedia.org/wikipedia/commons/0/0d/PEM_fuelcell.svg

from fluorine. Immobilised organic radicals were measured at the cathode side, which demarked the initiation of oxidative damage to the membrane. The yield of radicals was significantly greater for the fluorine-free membrane than for Nafion. Free radical intermediates were trapped at the anode which are involved in the fuel-oxidation process but evidence of membrane degradation was absent[143]. Another group has undertaken an investigation of the stability of polymer membranes, principally for use in PEM fuel cells. To whit, the comparative robustness of Nafion, stabilised Nation (StNafion), and 3 M and Aquivion membranes toward attack by the hydroxyl radical, $\cdot OH$ was assessed using aqueous dispersions of the polymers at 300 K. Two types of adducts were detected in all dispersions: DMPO/OH and DMPO/CCR, a spin-adduct of polymer-derived carbon-centred radicals (CCRs). The results indicated that StNafion was more robust than Nation, while the 3 M and Aquivion polymers were significantly the most stable. It would appear that the absence of the ether group and of the tertiary carbon in the side chain is the cause of the greater stability of these ionomers. A competition kinetics approach was used to determine the reaction rate constant of Ce(III) with $HO\cdot$ radicals to yield $k = 2.8 \times 10^8\,M^{-1}\ s^{-1}$, which agrees excellently with that $3 \times 10^8\,M^{-1}\ s^{-1}$ given in the literature[144]. A fuel-cell (FC) running in the cavity of an ESR spectrometer was used to

monitor the formation of $HO\cdot$ and $HOO\cdot$ radicals, $H\cdot$ and $D\cdot$ atoms, and radical fragments derived from the Nafion membrane, using DMPO as a spin-trap. Measurements were made with H_2 or D_2 at the anode and O_2 at the cathode. The FC was operated at 300 K with a membrane-electrode assembly (MEA) based on Nafion 117 with a Pt catalyst, causing closed and open circuit voltage conditions, CCV and OCV, respectively. Both anode and cathode chemistry was investigated. The DMPO/OH adduct was detected only at the cathode for CCV operation, implying that $\cdot OH$ radicals were produced from H_2O_2 formed electrochemically via the two-electron reduction of oxygen. The DMPO/OOH adduct, which was detected in this study for the first time in a FC, appeared at both the cathode and the anode for OCV operation, and at the cathode after an operating time of >2 h. A mechanism is proposed in which $HOO\cdot$ radicals are generated electrochemically at the cathode ($HO\cdot + H_2O_2 \rightarrow H_2O + HOO\cdot$) and at the anode from hydrogen atoms and crossover oxygen ($H\cdot + O_2 \rightarrow HOO\cdot$). DMPO adducts of $H\cdot$ atoms and $D\cdot$ atoms were detected at the anode and cathode sides, for CCV and OCV operation. The detection of $H\cdot$ and $D\cdot$ atoms is significant in that these species are sufficiently reactive to abstract F-atoms from the tertiary carbon in the polymer membrane chain, leading to chain fragmentation, rather in the manner that ionizing radiation ''unzips'' the C—C backbone of polytetrafluoroethylene (PTFE) by forming initial carbon-centred radicals. CCR adducts were detected at the cathode after CCV FC operation; while weak signals from CCR adducts were also detected at the anode. Since the only component in the FC that could provide CCRs is the Nafion membrane, their presence indicates membrane fragmentation. In conclusion, the operation of a FC has been shown to include such actions as gas-crossover, surface-reactions at the catalyst, and it is conceivable that reactive $H\cdot$ or $D\cdot$ atoms attack the membrane. Since the latter do not occur in *ex situ* laboratory experiments it appears that different mechanisms may pertain in the real *in situ* case[145]. A study has been made by another group using EPR to monitor radical-induced degradation of partially fluorinated aromatic model compounds for fuel cell membranes[146]. A detailed investigation has been reported of the microscopic viscosity, ordering and polarity in Nafion membranes containing methanol-water mixtures, using Tempone as a spin-probe[147]. A related issue to the use of fuel cells, particularly of the PEM type intended for hydrogen as the ''fuel'', is the storage of hydrogen itself for which various materials have been explored including zeolites, but without success in

meeting the stringent requirements of either volumetric or weight density in respect to the volume or mass of the fuel-tank. For commercial applications, an acceptable energy density for a hydrogen storage tank is deemed to be that it can efficiently hold an amount of hydrogen equal to 6.5 wt% of the weight of the tank and 62 kg H_2/m^3 in terms of volume. However, although investigations of hydrogen storage methods have been carried out for over 30 years, there has been no single one developed which fulfils these demanding criteria. Some approaches meet the weight target, but occupy unsatisfactorily large volumes (tanks of compressed hydrogen gas) yet others achieve the volume target but not the weight ratio (metal hydride absorbents)[138]. A solid consisting of single-walled carbon nanotubes (SWCNTs) encapsulated by thin Pd layers onto a Pd substrate has been investigated as a novel material for hydrogen storage which shows a synergetic effect from a combination of the adsorptive affinities for hydrogen of Pd and the SWCNTs. A high effective H_2 pressure is provided from the highly H-loaded massive Pd substrate into a small fraction of deposited SWCNT which allowed the attainment of a net capacity of 8 – 12 wt%. H_2. ESR measurements established that the Pd-C_x-complexes which formed at the openings of the SWCNTs can be considered as adsorption sites for H_2, providing both a high gravimetric capacity ($H/C > 1$) and low hydrogen binding energy in the Pd encapsulated SWCNT, thus the gas can be released for application, to a fuel cell[148].

18.2 Methane hydrate

Methane hydrate[137] (Figure 10) is formed when methane gas and water are brought together under suitable conditions of low temperature and elevated pressure, such that an ''ice'' type structure is formed containing methane molecules in considerable quantity. The solid material can hold 164 times its own volume of methane. The temperature at which methane-hydrate is stable depends on the prevailing pressure. For example, at 0°C, it is stable under a pressure of about 30 atmospheres, whereas at 25°C, nearer 500 atmospheres is needed to maintain its integrity. The occlusion of additional gases within the ice structure tends to add stability, whereas the presence of salts (NaCl, as from sea water) requires higher stabilising pressures. Appropriate conditions of temperature/pressure exist on Earth in the upper 2000 metres of sediments in two regions: (i) in permafrost at high latitudes in polar regions where the surface temperatures are very low (below freezing), and

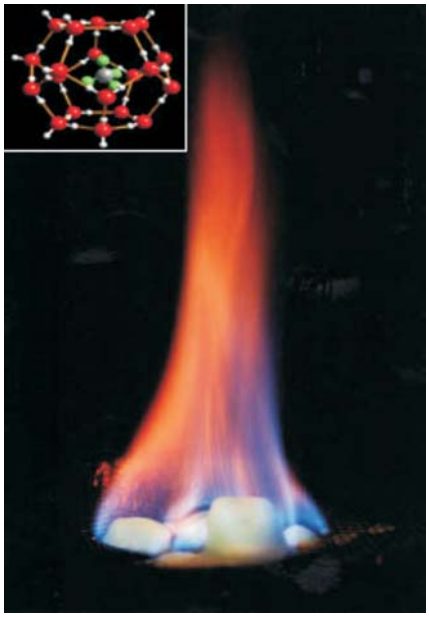

Figure 10 *"Burning ice". Methane, released by heating, burns; water drips. Inset: clathrate structure (University of Göttingen, GZG. Abt. Kristallographie). Source: United States Geological Survey. http://upload.wikimedia.org/wikipedia/commons/0/03/Burning_hydrate_inlay_US_Office_Naval_Research.jpg*

(ii) submarine continental slopes and rises, where not only is the water cold (around freezing), but the pressures are high (greater than 30 atmospheres), since the pressure increases by one atmosphere for every 10 metres of depth. Thus, in polar regions, methane-hydrate is found where temperatures are cold enough for onshore and offshore permafrost to be present. In offshore sediments, methane-hydrate is found at water depths of 300–500 m, according to the prevailing bottom-water temperature. There are reported cases where ''chunks'' of methane-hydrate break-loose from the sea bottom and rise to the surface, depressurizing and warming, where they ''fizz'' from the release of methane as they decompose to the gas/water state. There are manifold and widely disputed estimates of exactly how much methane-hydrate there is. However, a figure of 10^{16} cubic metres (m^3) of methane gas occluded within the entire global deposits of this material is probably a reasonable estimate. One estimate[149] puts the total at nearly $10^{19}\,m^3$, but this is the only one of such magnitude. Notwithstanding, the quantities of methane-hydrate are vast, and in view of this, it is thought that it might provide a potentially

significant energy source, probably at least four times the entire reserve of fossil fuels (gas, oil, coal) known (estimated). As ''peak oil'' [150] bares its teeth, the possibility appears increasingly attractive. However, the actual extraction of methane from this source is beset by a number of difficulties: low permeability of sediments, which restrict the actual flow of methane; lack of sustained interest from the oil/gas industry (though this may well change, *vide supra*, according to rising pressures of demand upon the existing limited resource); current limited gas-industry infrastructure at methane-hydrate locations; and the fact that no good field example has yet been demonstrated of the successful production of methane from its gas-hydrate. All these considerations score on the negative side as far as methane-hydrate becoming a serious fuel source is concerned. It seems clear that in a warming world (for whatever reason), methane will be released in increasing quantities, from warming permafrost, thus augmenting global warming. Disturbances on the sea bed may also cause the decomposition of methane-hydrate. It is known that drilling into methane hydrate poses a hazard to oil prospecting operations, and it is also thought that decomposition of methane hydrate with an eruption of methane could trigger a tsunami. More catastrophically, it is believed by some that world-scale eruptions of methane from these ''ice'' deposits can have triggered climate–CHange (global warming) on a cataclysmic level, most notably the Permian–Triassic (P–T or PT) extinction event, sometimes informally called the Great Dying, which was an extinction event that occurred approximately 252 million years ago, forming the boundary between the Permian and Triassic geologic periods. It was the Earth's most severe extinction event, with about 90% of all marine species, and 70% of terrestrial vertebrate species going extinct. For some time after the event, fungal species were the dominant form of terrestrial life, and perhaps this is once again the destiny for life on Earth.

In the context of the present review, we note that methane hydrates may be investigated using ESR, on the basis that methyl radicals are induced by exposure to ionizing radiation and which remain trapped within the ice matrix, so long as the overall structural integrity of the material is preserved. However, on raising the temperature, structural changes occur for which energetics can be determined according to diffusion and combination of the radical species resulting in reduction and ultimately loss of the intitial ESR signal. In a series of measurements made in the temperature range 210–260 K, the methyl radical signal was found

to decay according to second-order kinetics by combination to form ethane. However, two quite separate temperature-dependent processes were observed with respective activation energies of $20.0 \pm 1.6\,\text{kJ mol}^{-1}$ for the lower temperature range 210–230 K and $54.8 \pm 5.7\,\text{kJ mol}^{-1}$ for the higher temperature range 235–260 K. The former value accords with the enthalpy change of methane hydrate dissociation into ice and gaseous methane, while the latter agrees well with the enthalpy change into liquid water and gaseous methane. It is clear therefore that methane hydrates dissociate into liquid (supercooled) water and gaseous methane in the temperature range 235–260 K[151]. The approach was extended to a sample of natural methane hydrate collected from the deep ocean floor in Ocean Drilling Program (ODP) Leg 164. Following γ-irradiation, ESR signals from the methyl radical were observed along with those from an unidentified radical species. As expected, the decay energetics and thermal stability were very similar to those from the synthetic sample, but the signal intensity was about one eightieth of that from the synthetic sample, because the methane hydrate had partially lost methane gas and been converted to ice. It is proposed that the intensity of the ESR signal from the methyl radical detected following exposure to γ-rays might be used to estimate the amount of methane hydrate in a sample mixed with ice[152]. ESR measurements were also made on a sample of ethane hydrate, which had been exposed to γ-radiation. ESR signals were recorded from the ethyl radical ($g = 2.0031 \pm 0.0005$, $A_{\alpha\perp} = 2.2 \pm 0.1\,\text{mT}$, $A_{\alpha\|} = 2.5 \pm 0.1\,\text{mT}$, $A_{\beta} = 2.7 \pm 0.1\,\text{mT}$) and atomic hydrogen ($g = 2.0026 \pm 0.0005$, $A = 50.5 \pm 0.1\,\text{mT}$). From the results of ESR analysis and gas mass spectroscopy, it is concluded that the ethyl radical decays into butane by dimerisation in the first-order reaction in the temperature region of 250–265 K. The activation energy of the decay reaction is $73.1 \pm 6.3\,\text{kJ mol}^{-1}$, which is close to the dissociation enthalpy for the conversion of ethane hydrate to liquid water and gaseous ethane[152]. It is concluded therefore that ethane hydrate does not dissociate into ice but supercooled water, at least in this temperature range, which is similar to the dissociation behaviour of methane hydrate as determined previously[151].

18.3 ESR of coal

ESR has also been applied to study the quality of coal in which complex paramagnetic centres have been found. Samples of flame coal (71.4 wt% C), medium-rank coal (85.6 wt% C) and anthracite

(94.9 wt% C) were analysed along with macerals (exinite, vitrinite, inertinite) of coals containing 73.8 wt% C and 85.6 wt% C. It was found that the spin-concentration increased both in coal and macerals as the carbon content increases. Four groups of paramagnetic centres were identified in medium-rank coal, but only two groups in flame coal and anthracite. The ESR spectrum of medium-rank coal is a superposition of two broad and two narrow lines. Both broad and narrow lines were recorded from flame-coal, and two narrow lines in anthracite. Two kinds of paramagnetic centres with broad lines and one group with narrow lines exist in exinite and vitrinite from medium-rank coal. Two different broad ESR signals were detected for macerals from low-coalificated coal. The most complex paramagnetic centres were found in medium-rank coal samples. Broad ESR lines were not observed from the higher coalificated samples, anthracite and inertinite from medium-rank coal while narrow lines are not recorded in the ESR spectra of low-coalificated macerals. Strong dipolar interactions and rapid spin-lattice relaxation processes are characteristic for paramagnetic centres with broad lines. Strong exchange interactions and short spin-lattice relaxation times were measured for paramagnetic centres with the narrowest ESR signals[154].

18. ESR of photovoltaic systems

ESR and spectroelectrochemical studies of poly(3,4-ethylenedioxythiophene) (PEDOT) have been carried out. It was found that concentrations of paramagnetic centres in PEDOT vary from 0.02 spins per mer in the dedoped state to a maximum of 0.12 spins per mer at a doping level of 0.15 e^-/mer, which corresponds to 1 spin per *ca* 8.5 meric units. Such high spin-concentrations indicate that polarons are a major charge carrier group in PEDOT, which contrasts with observations made for other members of polythiophene family. Moreover, polarons do not disappear at high doping levels of PEDOT but rather their numbers decline gradually down to 0.08 spins per mer at a maximum doping level of 0.55 e^-/mer as met in this study. Based on information about concentrations of spins and polymer doping charges, concentrations of bipolarons have been evaluated as a function of doping level from which it appears that bipolaron formation begins at a doping level of *ca* 0.06 e^-/mer[155]. The magnetic susceptibility of solutions and powders of polyaniline was measured by ESR in the temperature range 123–423 K, and can be described by the integral of the susceptibility of the polymer fragments in the triplet state over the

singlet-triplet energy level splitting. Mainly, the dependences can be described in terms of the sum of the temperature-independent susceptibility and the Curie-law susceptibility. In some cases, by comparing the calculated and experimental dependences, the length of the fragments L can be determined. A similar analysis can be applied to other conducting polymers[156]. So-called charge transfer complexes (CTCs) in plastic solar cell materials influence the properties of organic solar cells. In one study it is shown that CTCs can be captured by light-induced electron spin resonance (I-ESR) with a much higher sensitivity than is possible with conventional methods, such as photoinduced absorption spectroscopy. Thus, the I-ESR technique rendered possible the demonstration that CTC states exist by their direct excitation with low-energy photons in an organic polymer/fullerene blend and, also in hybrid blends of poly(3-hexylthiophene) and CdSe nanoparticles. Furthermore, the recombination kinetics are analysed and some discussion given of them[157].

19. ESR studies of ionic liquids

Being composed entirely of ions, ionic liquids were once mainly a province of electrochemists. Recently, however, it has become apparent that, *inter alia*, their lack of measurable vapour pressure characterises them as green solvents, and that a wide range of chemical reactions can be performed in them[158]. In one study, the spin-probes TEMPO, TEMPOL and CAT-1 (4-trimethylammonium-2,2,6,6-tetramethylpiperidine-1-oxyl) were used to investigate both the microviscosity and micropolarity of imidazolium-based ionic liquids. It was found that the mean rotational correlation times (r) obtained by detailed simulation of the X-band ESR spectra of TEMPO, TEMPOL and CAT-1 increase with increasing viscosity of the ionic liquid as expected, but the normal Stokes-Einstein behaviour is not found. It was noted that ther probe molecule jumped into the free volume of the ionic liquids by a non-thermally activated process, which is most surprising. The ^{14}N coupling constants show a micropolarity for the ionic liquids comparable with that for dichloromethane for TEMPO and with dimethyl sulfoxide for TEMPOL. The micropolarity monitored by CAT-1 is found to depend strongly on variations in the structure of the ionic liquid[159]. TEMPO, TEMPOL and CAT-1 were employed along with their ^{15}N variants (^{15}N-TEMPO and ^{15}N-TEMPOL-D_{17}) similarly as probes of microviscosity and micropolarity in ionic liquids. It was concluded that microviscosity effects according

to the Gierer-Wirtz theory may explain the spin-probe behaviour. On the basis of spin exchange effects measured using TEMPO, TEMPOL and CAT-1 dissolved in ionic liquids, it is concluded that there is a greater degree of aggregation in the case of the non-polar spin-probe TEMPO. Both isolated and aggregated species were observed for the more greatly polar probes TEMPOL and CAT-1[160].

20. ESR studies of organic matter and kerogen in regards to oil and gas formation

ESR has also been used as a guide to determine the maturation of organic matter and for kerogen typing in the North Sea. In early ESR analysis of North Sea wells, maturation of organic matter (OM) was expressed in terms of maximum palaeotemperature (MPT) based on North American calibrations that did not consider the influences of kerogen composition or overpressure. In the North Sea, the MPTs were anomalous in overpressured sequences and relative to other indices of OM maturation such as vitrinite reflectance, so the ESR method was abandoned there in geochemical studies. However, early empirical study of North Sea ESR data indicated that, in relation to functions that linked temperature and pore pressure, some ESR parameters were predictable without reference to MPTs. In order to re-evaluate ESR parameters as indices of OM maturation, the physical factors (temperature and pressure) which affect OM maturation were related in to the g-value and the spin concentration (Ng) (spin density) at six well locations in the northern North Sea. A third ESR parameter, W (line width), is not an effective guide to maturation levels due to its complex relationship to the physical factors and kerogen types. However, cross-plots of W *versus* ''g'' and Ng appear to be as effective as pyrolysis for kerogen typing. Levels of maturation investigated in the North Sea wells range through the equivalent vitrinite reflectance values of about 0.50–1.50%. The values of ''g'' and Ng have been differentiated for kerogen type, but undifferentiated values of ''g'' have also been studied. Regression analysis has shown that there are linear relationships between the ESR parameters ''g'' and Ng, and the physical factors present-day temperature (To), ''effective'' temperature (Te), and differential pressure (Pd). Correlation coefficients for both ''g'' (undifferentiated and differentiated) and Ng (differentiated) relative to the physical factors are high; the highest values are for ''g'' and Ng relative to Te and Pd ($r = -0.950$ for ''g'' differentiated or undifferentiated, $r = 0.944$–

0.976 for Ng differentiated, respectively). However, correlation coefficients were lower for ''g'' and Ng relative to To. More frequent high correlation coefficients and larger sample populations suggest that ''g'' (undifferentiated) is a more reliable index of OM maturation than Ng (differentiated). However, the estimation of levels of OM maturation is improved if both indices are used together. The ESR method appears to be effective both for estimating levels of OM maturation and for kerogen typing. It has a number of potential advantages over other geochemical methods: firstly, it is more sensitive for estimating OM maturation than most other methods; secondly, it can be used to analyse organic matter which is as old as Proterozoic; thirdly, it does not destroy the samples analysed[161].

21. ESR applied to extraterrestrial samples

ESR measurements were made on samples collected from the Moon during the Apollo 11 and Apollo 12 missions. It was Apollo 11 that first landed humans on the lunar surface on July 20 1969. Apollo 12's mission was to prove that a ''pin-point'' landing was possible, since Apollo 11 had actually landed some 4 kilometers away from its intended target, and landing accuracy was important for taking samples to compile a geological map of the Moon. A broad signal was recorded centred at $g = 2.09 \pm 0.03$ and assigned to ferromagnetic centres, specifically from small metallic iron particles. In some samples, weak signals were also observed from $Mn(H_2O)_6^{2+}$ in which the metallic iron content is either low or partially removed. No signals were detected from either free electrons or holes, which might be expected as indicative of radiation damage, nor from Ti^{3+} [162]. S-type asteroids are thought to be parent bodies of ordinary chondrites and yet their reflectance spectra are different from ordinary chondrites. It is thought that the source of the difference is space weathering, where impacts from high-velocity dust particles change the optical properties of the uppermost regiolith surface of asteroids. By means of a laser whose pulse-duration and energy were chosen to match real conditions of heating by dust impacts, similar optical changes can be induced. Nanophase iron particles were detected by ESR, which are considered as the essential result of space weathering[163]. A detailed paper on space weathering essentially validates the idea that it is caused by metallic iron nano-particles smaller than the wavelength in ubiquitous vapour-deposited coatings on soil particle surfaces and inside agglutinates. The vapour is produced by both solar wind

sputtering and micrometeoric impact vapourisation and injected preferentially downward into the porous regiolith. The iron is reduced by a physical process, the selective loss of oxygen that occurs during deposition of the vapour, and does not reqire heating, melting or a reducing environment (hydrogen). The single-domain iron particles are detected by ESR[164]. The 1976 Viking landers on Mars peformed a series of experiments in which soil samples were analysed for evidence of life. Although no biological responses were elicited, samples of soil from 10 cm beneath the surface on contact with water released oxygen in larger amounts than would be expected from a simple physical desorption. A sample of plagioclase feldspar was irradiated with UV light for 20 hours under a simulated Martian atmosphere, which caused the formation of superoxide radical anions according to ESR. It is proposed that it is the reaction between superoxide and water that is responsible for the liberation of oxygen in the Martian samples[165]. Another group has investigated this interesting topic. Their results show that when finely ground basaltic minerals are added to water, H_2O_2 is produced and in sufficient quantities to explain the Viking Lander results. It is proposed that reaction occurs between water and defects at the surface of mechanically pulverised minerals, in analogy with carcinogenic quartz dusts. It appears too that the yield of H_2O_2 is increased by dehydroxylation of the mineral surface, as is especially significant for dusts on the airless surface of the Moon. It is suggested that a significant health hazard might be posed by fine-grained basaltic dusts to astronauts visiting planetary bodies whose surfaces have been impacted to generate such materials[166]. The stability of radiation-induced radicals in solid H_2O and CO_2 was investigated from the point of view of using these materials for future ESR dating of outer planets, their satellites and comets in the solar system. The samples were irradiated at 77 K using a ^{60}Co γ-ray source and measured at several temperatures with ESR to derive an isothermal decay time for the signal intensity. By extrapolation of an Arrhenius plot, the lifetime of the defects was deduced at the ambient temperature of the outer planets, and their satellites: Uranus, Neptune, Pluto and Triton (the largest moon of Neptune). The signals are stable over periods of years and it appears that by using a portable ESR with a lightweight Nd–Fe–B magnet it might prove possible to date remote samples in the solar system. In view of the nature of the outer planets (gas giants) it is thought that similar measurements on solid methane might prove worthwhile[167]. A search was made for ESR-based markers of the history and origin of the insoluble organic

matter (IOM) in extraterrestrial and terrestrial rocks. Three samples were taken of the IOM from carbonaceous chondrites, (Orgueil, Murchison and Tagish Lake meteorites) and three samples of cherts (microcrystalline silicate rock) containing microfossils ranging in age from 45 million years to 3.5 billion years. It was found that the organic matter in the meteorites (whose age is the age of the solar system) contains a high concentration of diradicaloid molecules with a diamagnetic ground state and a thermally accessible triplet state ($S = 1$). The latter is significant because such species are unknown in IOM of terrestrial origin. It is further shown that the ESR linewidth recorded from the IOM in cherts and coals decreases with the logarithm of the age of the material. The conclusion is drawn that the organic matter in the oldest cherts (3.5 billion years) has the same age as the silica matrix, and does not originate from contamination by bacteria[168]. Elsewhere, the nature of the diradicaloid species has been addressed. The macromolecular IOM from the Murchison and Orgueil meteorites is highly aromatic and contains organic radicals concentrated in microregions rather than the homogeneous distribution found in terrestrial samples. On the basis of the signal intensity increase found above 150 K (due to population of the $S = 1$ state), and electronic structure calculations made using extended Huckel and Density Functional methods, it was concluded that the diradicaloid species could be assigned to aromatic fusions of between 10 and 15 benzene rings, with two unpaired electron functions attached ($-CH_2\cdot$) in a quinoidal structure[169]. An important feature of meteoric IOM compared with terrestrial IOM is a systematic enrichment in deuterium, which is highly heterogeneous. It has been shown that organic radicals in the IOM constitute the D-rich carriers in the D-rich hotspots. The electronic structure of the radicals has been deduced from the measurement of the spin states S by transient nutation in pulsed-EPR. It is shown that these deuterium-rich radicals are dominated by biradicaloids (species with an $S = 0$ ground state and a thermally accessible $S = 1$ state) and biradicals (species with an $S = 1$ ground state) representing *ca* 61% and *ca* 31% of the radicals in the IOM of the Orgueil meteorite, respectively, while single radicals ($S = 1/2$) are present as only *ca* 8% of the total. In contrast, mature terrestrial IOMs contain almost exclusively $S = 1/2$ radicals. A structural model is proposed, in which the occurrence of dominant biradicaloids and biradicals is a direct consequence of the structure of the IOM, which consists of a network of small aromatic rings linked by branched and short aliphatic units. This implies that the formation of stable biradicaloids and biradicals by C–H

breaking and their deuterium enrichment occurs after the formation of the IOM in the primitive solar system. The idea therefore is reinforced that the formation of the IOM and the deuterium-rich hotspots are the product of ion chemistry in the solar disk[170].

22. ESR in food and nutraceutical research

An ESR-based method for the quantitative/qualitative determination of the purity of cane sugar has been proposed. The sucrose radical is produced when sugar is pulverised, the concentration of which increases as the particle size decreases. It is found that the ESR peak area for the radical increases linearly as the sucrose content of the material (refined sugar, plantation white sugar, soft brown sugar and raw sugar were used as samples)[171]. A review has been published on applications of ESR in nutraceutical and food research, in particular to determine the free radical scavenging capacity, oxidative stability evaluation and Cu^{2+} chelating capacity of foodstuffs. The potential of the ESR spin-label oximetry technique is exemplified[1] in the determination of lipid peroxidation and oxygen diffusion–concentration products in liposomes, oxygen transport and depletion, along with membrane structure and dynamic properties. The use of ESR in determining whether foods including meat, fruits, vegetables, spices, cereal grains, and oil seeds had been irradiated was surveyed. In a final section an account was given of the investigation of microstructural changes, phase transitions and viscosity changes during food formulation, processing, and storage, along with the potential of the method to investigate the radio-stability of food components[172]. The spin-probe technique has been applied to foodstuffs by Sutcliffe and his coworkers[173–175]. The spin-probe 1,1,3,3-tetramethylisoindolin-2-yloxyl (TMIO) and its sodium sulfonate salt derivative, sodium 1,1,3,3-tetramethylisoindolin-2-yloxyl-5-sulfonate (NaTMIOS), were used to monitor the microviscosity changes of water during starch gelatinization. In cereal starch, which contains mostly A-type polymorphs, evidence was found for the amylopectin and amylase regions: the latter exhibited a phase transition at about 55°C and a substantial increase in the microvoscosity was noted on cooling[172]. The same approach was also used to study changes in micro-viscosity in the aqueous and lipid phases of flour dough during heating and subsequent cooling. Hence, starch gelatinisation could be studied in detail and it was shown that the process results in a fall in the dielectric constant of the material[174]. Another foodstuff so investigated is ice-cream. Usin the TMIO probe, it was found that

when ice-cream is cooled, the fat phase is composed of a mixture of solid and liquid fat down to a temperature of *ca* $-60°C$. By means of the water-soluble probe NaTMIOS, it was found that the aqueous phase changes entirely from the solid to the liquid within 1°C of $-18°C$. On cooling further to $-24.7°C$, and then allowing the sample to warm-up to $+25°C$, the rotational correlation times of the latter probe were slow to recover their original values. For the lipid phase, a value of 65.7 ± 2.0 ps was obtained for the rotational correlation time determined from the B parameter along with an activation enthalpy of 32.5 ± 0.9 kJ mol^{-1}. These values are typical of those expected to be found in the type of fat used to make ice-cream. The water phase gave correspondiong values of 32.2 ± 0.5 ps and 24.5 ± 0.4 kJ mol^{-1}, which are as expected for a sucrose concentration of 24%[171].

References

1. Rhodes, C.J. (2011) *Sci. Prog*., **94**, 16.
2. Yordanov, N.D. and Lubenova, S. (2000) *Anal. Chim. Acta*, **403**, 305.
3. Rhodes, C.J., Tran, T.T. and Morris, H. (2004) *Spectrochim. Acta, Part A*, **60**, 1401.
4. Yordanov, N.D., Lubenova, S. and Sokolova, S. (2001) *Atmos. Environ*., **35**, 827.
5. Yordanov, N.D., Mladenova, B. and Petkov, P. (2002), *Anal. Chim. Acta*, **453**, 155.
6. Yordanov, N.D. and Lubenova, S. (2000) *Anal. Chim. Acta*, **403**, 305.
7. Fox, M.A. and Dulay, M.T. (1993) *Chem. Rev.*, **93**, 341.
8. Serone, N. (1994) *Res. Chem. Intermed*., **20**, 953.
9. Ollis, D.F. and Al-Ekabi, H. (eds), *Photocatalytic purification of water and air* (1993) Elsevier, Amsterdam.
10. Bahnemann, D. (2004) *Solar Energy*, **77**, 445.
11. Kraeutler, B. and Bard, A.J. (1978) *J. Am. Chem. Soc*., **100**, 2239.
12. Frank, S.N. and Bard, A.J. (1977) *J. Phys. Chem*., **81**, 1484.
13. Grela, M.A., Coronel, M.E.J. and Colussi, A.J. (1996) *J. Phys. Chem*., **100**, 16940.
14. Schwarz, P.F. *et al*. (1997) *J. Phys. Chem. B*, **101**, 7127.
15. Barrer, R.M. (1978) *Zeolites and Clay Minerals*, Academic Press, London.
16. Karger, J. and Ruthen, D.M. (1992) *Diffusion in Zeolites*, Wiley, New York.
17. Rhodes, C.J. (2010) *Sci. Prog*., **93**, 223.
18. *Restoration of environments with radioactive residues* (2000) International Atomic Energy Agency, Vienna.
19. Rhodes, C.J., Reid, I.D. and Zimmermann, U. (2002) *J. Chem. Soc., Chem. Comm*., 1092.
20. Mazzoleni, F., Ottaviani, M.F., Romanelli, M. and Martin, G. (1988) *J. Phys. Chem*., **92**, 1953.
21. http://igatur-archive.library.uu.nl/dissertations/2003-0325-143241/inhoud.htm
22. Okazki, M. and Toriyama, K. (2005) *J. Phys. Chem. B*, **109**, 20068.
23. Okazki, M. and Toriyama, K. (2005) *J. Phys. Chem. B*, **109**, 13180.
24. Okazki, M. and Toriyama, K. (2007) *J. Phys. Chem. B*, **111**, 9122.
25. Okazaki, M., Jin, P., Ohta, K. and Toriyama, K. (2009) *J. Phys. Chem. C*, **113**, 11086.
26. Okazaki, M., Seelan, S. and Toriyama, K. (2009) *App. Magn. Reson*., **35**, 363.
27. Liu, W., Komaguchi, K., Shiotani, M., Michalik, J. and Lund, A. (2000) *Phys. Chem. Chem. Phys*., **2**, 2515.

28. Liu, W., Shiotani, M., Michalik, J. and Lund, A. (2001) *Phys. Chem. Chem. Phys*., **3**, 3532.
29. Liu, W., Yamanaka, S., Shiotani, M., Michalik, J. and Lund, A. (2001) *Phys. Chem. Chem. Phys*., **3**, 1611.
30. Rhodes, C.J. (1991) *Trans. Faraday Soc*., **81**, 3179.
31. Liu, W. *et al*. (2003) *App. Magn. Reson*., **24**, 285.
32. Yahiro, H., Lund, A. and Shiotani, M. (2004) *Spectrochimica Acta Part A*, **60**, 1267.
33. Biglino, D. *et al*. (1999) *Phys. Chem. Chem. Phys*., **1**, 2887.
34. Li, H. *et al*. (1999) *Micropor. Mesopor. Mat*., **30**, 275.
35. Hirano, T. *et al*. (1999) *J. Am. Chem. Soc*., **121**, 7170.
36. Lem, G. and Turro, N.J. (2000) *Chem. Comm*., 393.
37. Turro, N.J. *et al*. (2002) *J. Org. Chem*., **67**, 2606.
38. Liu, Z. *et al*. (2004) *J. Phys. Chem. A*, **108**, 8040.
39. Moscatelli, A. (2008) *J. Am. Chem. Soc*., **130**, 11344.
40. Doetschman, D.C. and Thomas, G.D. (1998) *Chem. Phys*., **228**, 103; Rhodes, C.J. to be published.
41. Gardner, C.L. and Weinberger, M.A. (1970) *Can. J. Chem*., **48**(8), 1317; Rhodes, C.J. to be published.
42. Rhodes, C.J. (2007) *Annu. Rep. Prog. Chem. Sect. C: Phys. Chem*., **103**, 287.
43. Symons, M.C.R. (1996) *Free Rad. Biol. Med*., **6**, 831.
44. Tanaka, Y., Zhang, Q. and Saito, F. (2004) *J. Mater. Sci*., **39**, 5497.
45. McMillen, D.F. and Golden, D.M. (1982) *Ann. Rev. Phys. Chem*., **33**, 493.
46. Lankamp, H., Nauta, W.Th. and MacLean, C. (1968) *Tetrahedron Letters*, **9**, 249.
47. Dadali, A.A.. Lastenko, I.P., Aksenkov, V.V. and Ivanon, A.N. (1993) *Russ. J. Phys. Chem*., **67**, 166.
48. Maeda, K. and Huyashi, (1970) *T. Bull. Chem. Soc. Jpn*., **43**, 429.
49. Mori, Y. *et al*. (1996) *Bull. Chem. Soc. Jpn*., **69**, 2355.
50. Urbanski, T. (1967) *Nature*, **216**, 577.
51. Varentsov, E.A., Bystrikov, A.B. and Karpal, V.M. (1988) *Russ. J. Phys. Chem*., **62**, 1089.
52. Varentsov, E.A. and Khrustalev, Yu.A. (1995) *Russ. Chem. Rev*., 783.
53. Tipikin, D.S., Lazarev, G.G. and Lebedev, Ya.S. (1993) *Russ. J. Phys. Chem*., **67**, 159.
54. Tipikin, D.S., Lebedev, Ya.S. and Rieker, A. (1997) *Chem. Phys. Lett*., **272**, 404.
55. Finlayson-Pitts, B.J. and Pitts, Jr. J.N. (2000) *Chemistry of the upper and lower atmosphere*, Academic Press, San Diego.
56. Mihelcic, D., Musgen, D.K.P., Patz, H.W. and Volz-Thomas, A. (1993) *J. Atmospheric. Chem*., **16**, 313.
57. Burns, D.T., Salem, M.A., Baxter, R.I. and Flockhart, B.D. (1986) *Anal. Chim. Acta*, **183**, 281.
58. Loktev, M.I. and Slinkin, A.A. (1976) *Russ. Chem. Rev*., **45**, 807.
59. Yordanov, N.D. (1999) In: Spurny, K.R. (ed.), *Analytical chemistry of aerosols*, Lewis Publishers, Boca Raton, p. 197.
60. Yamanaka, C., Matsuda, T. and Ikeya, M. (2005) *App. Radiat. Isotop*., **62**, 307.
61. Xie, Z., Blum, J.D., Utsunomiya, S., Ewing, R.C., Wang, X. and Sun, L. (2007) *J. Geophys. Res*., **112**, D02306, doi: 10.1029/2006JD007247.
62. Schnitzer, M. (1990) In: MacCarthy, P., Clapp, C.E., Malcolm, R.L. and Bloom, P.R. (eds), *Humic substances in soil and crop sciences*, American Society of Agronomy, Inc; Soil Science Society of America, Madison, p. 70.
63. Lakatos, B., Tibai, T. and Meisel, J. (1977) *Geoderma*, **19**, 319.
64. Cheshire, M.V., Berrow, M.L., Goodman, B.A. and Mundie, C.M. (1977) *Geochem. Cosmochim. Acta*, **41**, 1131.
65. Boyd, S.A., Sommers, L.E., Nelson, D.W. and West, D.X. (1981) *Soil Sci. Soc. Am. J*., **45**, 745.
66. Witwicki, M. *et al*. (2008) *Chem. Phys. Lett*., **462**, 300.
67. Jezierski, A. *et al*. (2002) *Spectrochimica Acta A*, **58**, 1293.

68. Bayer, C., Martin-Neto, L., Miclniczuk, J., Pillon, C.N. and Sangoi, L. (2001) *Soil Sci. Soc. Am. J.*, **65**, 1473.
69. Regenerative organic farming: a solution to global warming. http://www.rodaleinstitute.org/files/Rodale_Research_Paper-07_30_08.pdf
70. Dumestre, A., McBride, M. and Baveye, P. (2000), *Environ. Sci. Technol*., **34**, 1259.
71. Kale, S.P., Murthy, N.B.K. and Raghu, K. (2001) *Chemosphere*, **44**, 893.
72. Jezierski, A., Bylinska, E. and Seaward, M.R.D. (1999) *Atmospheric Environment*, **33**, 4629.
73. Yordanov, N.D., Novakova, E. and Lubenova, S. (2001) *Anal. Chim. Acta*, **437**, 131.
74. Rhodes, C.J. (ed.), *Toxicology of the human environment - the critical role of free radicals* (2000), Taylor and Francis, London.
75. Gulumian, M., Bhoolia, D.J., Theodorou, P., Rollin, H.B., Pollak, H. and Vanwyk, J.A. (1993) *S. Afr. J. Sci*., **89**, 405.
76. Gulumian, M. *et al*. (1993) *J. Inorg. Biochem*., **50**, 133.
77. Gulumian, M., Nkosibomvu, Z.L., Channa, K. and Pollak, H. (1997) *Environ. Health Perspec*., **105**, 1041.
78. Ghio, A.J., Kadiiska, M.B., Xiang, Q.H. and Mason, R.P. (1998) *Free Rad. Biol. Med*., **24**, 11.
79. Ottaviani, M.F. and Venturi, F. (1996) *J. Phys. Chem*., **100**, 265.
80. Dalal, N.S., Newman, J., Pack, D., Leonard, S. and Vallyathan, V. (1995) *Free Rad. Biol. Med*., **18**, 11.
81. Shi, X.L. *et al*. (1995) *J. Toxicol. Env. Health*, **46**, 233.
82. Shi, X.L., Flynn, D.C., Porter, D.W., Leonard, S.S., Vallyathan, V. and Castranova, V. (1997) *Annals Clin. Lab. Sci*., **27**, 365.
83. Hideg, E. and Vass, I. http://www.photobiology.com/v1/hideg/index.htm
84. Van Bilsen, D.G.J.L. and Hoekstra, F.A. (1993) *Plant Physiol*., **101**, 675.
85. Van Bilsen, D.G.J.L., Hoekstra, F.A., Crowe, L.M. and Crowe, J.H. (1994) *Plant Physiol*., **104**, 1193.
86. Buitlink, J., Walters-Vertucci, C., Hoekstra, F.A. and Leprince, O. (1996) *Plant Physiol*., **111**, 235.
87. Leprince, O. and Walters-Vertucci, C. (1995) *Plant Physiol*., **109**, 1471.
88. Buitlink, J., Walters, C., Hoekstra, F.A. and Crane, J. (1998) *Physiol. Plant*, **103**, 145.
89. Sun, W.Q. (1997) *Ann. Bot*., **79**, 291.
90. Hemminga, M.A. and Van den Dries, I.J. (1998) Biological magnetic resonance, Vol. 14. In: Berliner, L.J. (ed.), *Spin labelling: The Next Millenium*, Plenum, New York, p. 1.
91. Buitlink, J., Claessens, M.M.A.E., Hemminga, M.M. and Hoekstra, F.A. (1998) *Plant Physiol*., **118**, 531.
92. Buitlink, J., Hoekstra, F.A. and Hemminga, M.A. (2000) *Seed Science Res*., **10**, 285.
93. Batchelor, S.N. (1999) *J. Phys. Chem. B*, **103**, 6700.
94. Klemm, D. *et al*. (1998) *Comprehensive cellulose chemistry*, Vol. 1, Wiley-VCH, Weinheim.
95. Scheuermann, R., Roduner, E. and Batchelor, S.N. (2001) *J. Phys. Chem. B*, **105**, 11474.
96. Ottaviani, M.F., Retini, G., Cangiotti, M., Mangani, F. and Segre, U. (2002) *Spectrochim. Acta A*, **58**, 1129.
97. Ikeya, M. (1988) *Magn. Reson. Rev.*, **13**, 91.
98. Grun, R. (1989) *Quarternary International*, **1**, 65.
99. Grun, R. (1987) In: *Chronometric dating in archeology*, Plenum Press, New York, p. 217.
100. Grun, R. (2000) In: Ellis, L. (ed.), *Archaeological method and theory - an Encyclopedia*, p. 174.
101. Curnoe, D., Grun, R., Taylor, L. and Thackaray, F. (2001) *J. Human Evolution*, **40**, 379.
102. Grun, R. and Beaumont, P. (2001) *J. Human Evolution*, **40**, 467.
103. Thorne, A. *et al*. (1999) *J. Human Evolution*, **36**, 591.
104. Turney, C.S.M. *et al*. (2001) *Quarternary Research*, **55**, 3.

105. Blackwell, B.A.B. *et al*. (2010) *Health Phys*., **98**, 417.
106. Blackwell, B.A.B. *et al*. (2007) *Radiation Measurements*, **42**, Spec. Iss. (6–7), 1250.
107. Grun, R. and Stringer, C. (2000) *J. Human Evolut*., **39**, 601.
108. Grun, R. (2000) *Radiat. Meas*., **32**, 767.
109. Grun, R. (1998) *Radiat. Meas*., **29**, 177.
110. Vanhaelewyn, G., Callens, F. and Grun, R. (2000) *App. Radiat. Iso*., **52**, 1317.
111. Robertson, S. and Grun, R. (2000) *Radiat. Meas*., **32**, 773.
112. Grun, R. (2002) *Radiat. Meas*., **35**, 87.
113. Morsy, M.A. and Khaled, M.M. (2002) *Spectrochim. Acta A*, **58**, 1271.
114. Rhodes, C.J. (2010) *Chem. Ind*., December 20th.
115. Brueckner, A. (2007) *Adv. Catalysis*, **51**, 265.
116. Stoesser, R. (2010) *J. Am. Chem. Soc*., **132**, 9873.
117. Li, G. *et al*. (2008) *J. Am. Chem. Soc*., **130**, 5402.
118. Livraghi, S. *et al*. (2007) *Res. Chem. Interm*., **33**, 739.
119. Zhang, J., Xiao, L., Cong, Y. and Anpo, M. (2008) *Topics in Catalysis*, **47**, 122.
120. Polyakov, N.E. *et al*. (2010) *J. Phys. Chem. B*, **114**, 14200.
121. Fittipaldi, M. *et al*. (2009) *J. Phys. Chem. C*, **113**, 6221.
122. Brusa, M.A., Di Iorio, Y., Churio, M.S. and Grela, M.A. (2007) *J. Mol. Catal.–Chemical*, **268**, 29.
123. Zhang, D.-D. *et al*. (2009) *J. Hazard. Mater*., **163**, 843.
124. Araujo, J.C. *et al*. (2007) *J. Nanosci. Nanotechnol*., **7**, 3643.
125. Liu, C.X. *et al*. (2007) *J. Adv. Oxidat. Technol*., **10**, 11.
126. Tryba, B., Gzerwinska, M. and Morawski, A.W. (2007) *RILEM Proceedings, PRO 2007*, **55** (*Photocatalysis, Environment and Construction Materials*), 235.
127. Bandos, T.J. and Ania, C.O. (2006) *Interface Science and Technology*, **7** (*Activated Carbon Surfaces in Environmental Remediation*), 159.
128. Scorzelli, R.B. (2008) *Clay Minerals*, **43**, 129.
129. Jerzykiewicz, M., Cwielag, I. and Jerzykiewicz, W. (2009) *J. Chem. Tech. Biotech*., **84**, 1196.
130. Piccinato, M.T., Guedes, C.L.B. and Di Mauro, E. (2009) *Appl. Magn. Reson*., **35**, 379.
131. Di Mauro, E., Guedes, C.L.B. and Piccinato, M.T. (2007) *Appl. Magn. Reson*., **32**, 303.
132. Cogo, S.L. *et al*. (2009) *Braz. J. Phys*., **39**, 31.
133. Senglet, N. *et al*. (1990) *Fuel*, **69**, 203.
134. Guedes, C. *et al*. (2003) *Marine Chemistry*, **84**, 105.
135. Uesugi, A. and Ikeya, M. (2001) *Jpn. J. Appl. Phys*., **40**, 2251.
136. Dickneider, T.A., Whelan, J.K. and Blough, N.V. (1995) *Org. Geochem*., **23**, 97.
137. Rhodes, C.J. (2007) *Ann. Rep. Prog. Chem. Sect. C: Physical Chemistry*, **103**, 287.
138. Rhodes, C.J. (2005) "*Energy Balance*" http://ergobalance.blogspot.com
139. Panchenko, A. *et al*. (2004) *Phys. Chem. Chem. Phys*., **6**, 2891.
140. Panchenko, A. *et al*. (2004) *J. Power Sources*, **127**, 325.
141. Rhodes, C.J. (2008) *Annu. Rep. Prog. Chem. Sect. C: Phys. Chem*., **104**, 81.
142. Rhodes, C.J. http://blogs.forbes.com/energysource/2011/02/01/endangered-elements-pose-threat-to-green-energy/
143. Panchenko, A., Aleksandrova, E. and Roduner, E. (2005) *Fudan Xuebao Ziran Kexueban*, **44**, 719.
144. Danilczuk, M., Perkowski, A.J. and Schlick, S. (2010) *Macromolecules*, **43**, 3352.
145. Danilczuk, M., Coms, F.D. and Schlick, S. (2009) *J. Phys. Chem. B*, **113**, 8031.
146. Schoenberger, F., Kerres, J., Dilger, H. and Roduner, E. (2009) *Phys. Chem. Chem. Phys*., **11**, 5782.
147. Lawton, J.S., Smotkin, E.S. and Budil, E.D. (2008) *J. Phys. Chem. B*, **112**, 8549.
148. Lipson, A.G. (2009) *Diamond Relat. Mater*., **18**, 984.
149. Dobrynin *et al*. (1981), *Long-term energy resources*, Pitman, Boston, pp. 727.
150. Rhodes, C.J. (2008) *Sci. Prog*., **91**, 317.

151. Takeya, K. *et al*. (2005) *J. Phys. Chem. B*, **109**, 21086.
152. Takeya, K., Tani, A., Yada, T. and Ikeya, M. (2005) *Appl. Radiat. Isot*., **62**, 371.
153. Takeya, K. *et al*. (2007) *Jpn. J. Appl. Phys*., **46**, 3066.
154. Pilawa, B. and Wieckowski, A.B. (2007) *Res. Chem. Intermed*., **33**, 825.
155. Domagala, W., Pilawa, B. and Lapkowski, M. (2008) *Electrochim. Acta*, **53**, 4580.
156. Kulikov, A.V., Komissarova, A.S., Shishlov, M. N. and Fokeeva, L.S. (2008) *Russ. Chem. Bull*., **57**, 324.
157. Witt, F., Kruszynska, M., Borchert, H. and Parisi, J. (2010) *J. Phys. Chem. Lett*., **1**, 2999.
158. Earle, M.J. and Seddon, K.R. (2000) *Pure Appl. Chem*., **72**, 1391.
159. Stoesser, R. *et al*. (2006) *J. Phys. Org. Chem*., **19**, 318.
160. Stoesser, R. *et al*. (2006) *Z. Phys. Chem*., **220**, 1309.
161. McTavish, R.A. (2003) *J. Pet. Geol*., **26**, 65.
162. Tsay, F.-D. and Cjan, S.I. (1971) *Proc. Second Lunar Space Conference*, **3**, 2515.
163. Kurahashi, E., Yamanaka, C., Nakamura, K. and Sasaki, S. (2002) *Earth Planets Space*, **54**, e5.
164. Hapke, B. (2001) *J. Geophys. Res*., **106**, 10039.
165. Yen, A.S., Kim, S.S., Hecht, M.H., Frant, M.S. and Murray, B. (2000) *Science*, **289**, 1909.
166. Hurowitz, J.A. *et al*. (2007) *Earth and Planetary Science Letters*, **255**, 41.
167. Tsukamoto, Y., Ikeya, M. and Yamanaka, C. (1993) *App. Radiat. Iso*., **44**, 221.
168. Gourier, D. *et al*. (2004) *Spectrochim. Acta A*, **60**, 1349.
169. Binet, L. *et al*. (2004) *Geochim. Cosmochim. Acta*, **68**, 881.
170. Delpoux, O. *et al*. (2011) *Geochim. Cosmochim. Acta*, **75**, 326.
171. Thamaphat, K., Limsuwan, P. and Meejoo, S. (2007) *Chin. Phys. Lett*., **24**, 3524.
172. Yu, L. and Cheng, Z. (2008) *Molecular Nutrition and Food Research*, **52**, 62.
173. Robertson, J.A. and Sutcliffe, L.H. (2005) *Magn. Reson. Chem*., **43**, 457.
174. Robertson, J.A., Sutcliffe, L.H. and Mills, E.N.C. (2006, *J. Agric. Food Chem*., **54**, 1427.
175. Gillies, D., Greenley, K.R. and Sutcliffe, L.H. (2006) *J. Agric. Food Chem*., **54**, 4943.